The Nucleus Mediates Mechanosensitive Reorganization of Epigenetically Marked Chromatin During Cardiac Maturation and Pathology

*Benjamin Seelbinder[1], Soham Ghosh[1], Alycia G. Berman[2], Stephanie E. Schneider[1], Craig J. Goergen[2], Sarah Calve[2], Corey P. Neu[1,]**

[1] Department of Mechanical Engineering, University of Colorado Boulder, Boulder (CO)

[2] Weldon School of Biomedical Engineering, Purdue University, West Lafayette (IN)

** Corresponding Author*

Keywords: Cardiac development, Mechanosensation, Chromatin Organization, Nucleus, Epigenetics, Substrate Mechanics, Hypertrophy

ABSTRACT

Mechanical stimuli are essential to guide cell differentiation, but little is understood about the underlying mechanisms. The nucleus is thought to integrate mechanical signals through complexes that physically connect the nucleoskeleton to the cytoskeleton and exposome; however, direct evidence of nuclear mechanosensation is sparse, and its role in guiding cell differentiation is unclear. Here we investigated changes in chromatin organization during cardiac development and disease, and analyzed how contraction-generated nuclear strains impacted chromatin reorganization. We found that contractile cardiomyocytes adopt a distinct nuclear architecture during development that was driven by the reorganization of H3K9me3-modified chromatin. Degenerative (stiff) mechanical environments that inhibited nuclear deformation abrogated the formation and maintenance of the cardiac nuclear architecture *in vitro* and *in vivo*, and promoted the reorganization of H3K27me3-modified chromatin instead. By generating high-resolution maps of intranuclear strains exerted during cell contraction, we further isolated that

tensile hydrostatic, but not shear or deviatoric, strains guided the rearrangement of H3K9me3-marked chromatin. Moreover, disruption of LINC (Linker of Nucleo- and Cytoskeleton) complexes inhibited chromatin reorganization, but not epigenetic regulation as observed in stiff environments. Subsequent analysis revealed further complementary mechanosensitive pathways in the cytoskeleton (e.g. via stretch of p130Cas located within the sarcomeric Z-disk) that regulate epigenetic mediators. Together, our findings provide a novel role for nuclear mechanosensation and show that environmental and contractile mechanics can influence cell differentiation through reorganization of epigenetically-modified chromatin via nuclear mechanosensitive pathways.

INTRODUCTION

The mechanics of cellular microenvironments play an important role in directing cell differentiation during development [1,2] and changes in mechanical properties due to acute trauma, chronic conditions, or genetic predispositions lead to cellular degeneration and result in a range of pathologies including cardiac hypertrophy [3,4]. Further, regenerative medicine aims to engineer suitable microenvironments to guide cell fates for enhanced tissue regeneration. However, little is known about the underlying mechanisms that facilitate cell differentiation in response to environmental cues.

The nucleus is thought to be an essential mechanosensitive organelle, as it is tightly connected to all parts of the cytoskeleton through LINC (Linker of Nucleo- and Cytoskeleton) complexes comprised of proteins that span the inner (SUNs) and outer (nesprins) nuclear membranes [5]. Studies on isolated nuclei demonstrated that the nucleus alone can respond to stretch; however, only when engaged via LINC complexes [6]. Mutations in LINC complex and

nuclear envelope proteins are linked to developmental disorders, particularly in mechanically active tissues such as cardiac and skeletal muscle [7,8]. In addition, recent studies found a direct link between nuclear architecture and cellular differentiation, suggesting that chromatin organization might be important for stable lineage commitment [9–11]. Chromosome locations are more similar between cells of the same type and, to a lesser degree, different cells within the same tissue [12]. The establishment of cell type-specific nuclear architectures during differentiation have been reported for plasma cells [13], neutrophil granulocytes [14], T-cells [15] and photoreceptor cells [16].

We hypothesized that environmental cues physically guide cell differentiation by directly influencing how the nucleus regulates chromatin organization and positioning. In addition, we sought to identify whether epigenetic mechanisms play a role in orchestrating chromatin rearrangements as it has been shown to mediate chromatin positioning [17]. Here we investigated the organization of chromatin in cardiomyocytes (CM) and documented the establishment of a distinct nuclear architecture during development which was abrogated in pathology models. We could identify and show that tensile hydrostatic strains, transferred from contracting sarcomeres to the nucleus via LINC complexes, guided the reorganization of H3K9me3-modified chromatin to establish this architecture. We could further discern that nuclear mechanosensation primarily functioned to reorganized while epigenetic-modification of chromatin appeared to be controlled by complementary mechanosensitive pathways within the sarcomeric Z-disk lattice.

RESULTS

CMs Adopt a Distinct Nuclear Architecture During Development

To study relationships between functional microenvironments, nuclear morphology, and chromatin organization, we first screened tissues known to undergo a broad range of mechanical challenges and with different stiffness properties in adult H2b-eGFP mice *in vivo* (**Fig. 1a**) [18]. While all cell types showed distinct nuclear architectures, the nuclei of cardiomyocytes CM nuclei had an elongated morphology, with a disproportional amount of chromatin at the nuclear periphery, and inner cavities that appeared almost void of chromatin. In contrast, cardiofibroblasts (CF), which shared an elongated nuclear morphology in the same force-generating mechanical microenvironment, showed a homogeneous distribution of chromatin throughout the nucleus. Analysis of late stage (E18.5) embryonic hearts revealed that the nuclear architecture observed in adult CMs was not present in embryonic CMs (**Fig. 1b**) suggesting that the mature nuclear phenotype forms postnatally when a sudden demand for increased cardiac output triggers CM maturation.

To analyze the formation of a mature nuclear phenotype during CM development, we harvested cardiogenic precursor cells (CPC) from late stage (E18.5) mouse embryo hearts and plated them on soft (13 kPa) PDMS substrates that matched the mechanical environment of adult hearts to prompt cardiac maturation [19–21]. CPCs initiated coordinated contractions within one day of culture. After two days, nuclear phenotypes still appeared diffuse with no distinctive accumulation of heterochromatin at the nuclear envelope (**Fig. 1c**). However, after four days, cells that developed contractile sarcomere fibers exhibited intranuclear cavities devoid of chromatin and an overall shift of chromatin towards the nuclear periphery, like mature CMs (**Fig. 1a)**. Interestingly, non-contractile cells continued to display a diffuse nuclear architecture more similar to mature CFs. These findings provided further support for a link between chromatin

organization and cell differentiation and showed that CMs form a cell type-specific nuclear architecture during maturation.

Substrate Stiffness Affects Expression of Histone Modifying Genes in CPCs

Embryonic CMs show poor contractile properties and inhibited maturation on substrates that are stiffer than the native environment [19,20]. To screen for epigenetic modifications that guide the establishment of the mature nuclear architecture in CMs, we performed a comparative RNAseq analysis of CPCs cultured on soft (13 kPa) or stiff (140 kPa) PDMS for four days. Of 63 detected histone-coding genes, 51 were more than 30% and 33 were more than 50% downregulated on stiff substrates, which indicated inhibited chromatin remodeling (**Fig. 2a and S1**). Gene ontology (GO) term enrichment analysis of differentially expressed ($p<0.2$) genes with the parent GO term *histone modification* (GO:0016570) revealed the child GO terms *histone methylation* (GO:0016571) and *histone acetylation* (GO:0016573) as significantly enriched ($p=1.30E-9$, $p=5.50E-6$, respectively). Closer investigation of histone methylating genes showed that H3K9 methylating (aka methyltransferases) genes *Ehmt1*, *Setdb1* and *Eed* were among the most downregulated for CPCs cultured on stiff substrates (**Fig. 2b, Supplementary Table 1**).

Methylation of H3K9 is associated with strong gene repression and chromatin condensation [22] and has been shown to be crucial during cardiac development [23] and maintenance [3]. PCR analysis of CPCs cultured on stiff compared to soft PDMS validated downregulation of H3K9 methylating enzymes as well as downregulation of cardiac transcription and structural markers while no change in gene expression was observed for H3K9 demethylase *Kdm3a* (**Fig. 2c**). Genes *Eed* and *Ezh2* are also associated with the methylation of H3K27, in addition to H3K9 (**Supplementary Table 1**). Similar to H3K9, methylation of H3K27 is also associated with gene repression and heterochromatin formation [22]; however, it has an opposing function

during cardiac development and needs to be repressed for cardiac differentiation [24]. In accordance, PCR data showed that H3K27 demethylase *Kdm6a* was downregulated while H3K27-specific methylase *Ezh1* remained unchanged. Overall, gene expression data validated that degenerative (stiff) environments abrogated chromatin remodeling and significantly downregulated H3K9 methylating enzymes in CPCs.

Reorganization of H3K9 Methylated Chromatin Precedes That of Overall Chromatin in Contractile CPCs

We observed chromatin reorganization towards the mature nuclear phenotype in CPCs during four-day *in vitro* cultures on soft (13 kPa) PDMS; however, only in contractile cells. To determine whether epigenetic modifications mediate chromatin reorganization towards the nuclear periphery during cardiac maturation, we analyzed the spatial distribution of H3K9me3 and H3K27me3 in the nucleus of contractile and non-contractile CPCs (**Fig. 3a**). To quantify the enrichment of chromatin towards the nuclear periphery, intensities of H2b-eGFP, as an indicator of overall chromatin localization, and both epigenetic markers were analyzed over the relative distance to the nuclear center (0=center, 1=periphery). A peripheral enrichment score was calculated as the ratio of the peripheral bin (0.85-0.95) divided by the center bin (0.05-0.15, **Fig. 3b-d**). Both contractile and non-contractile CPCs showed no peripheral enrichment of overall chromatin after two days in culture. However, on day four, overall chromatin was enriched at the nuclear border in contractile cells while enrichment was slightly decreased in non-contractile cells compared to day two. In contractile CPCs, the shift of overall chromatin was preceded by the enrichment of H3K9me3-marked chromatin towards nuclear border on day two, followed by a higher enrichment on day four.

Non-contractile CPCs showed no peripheral accumulation of H3K9me3-marked chromatin on either day; instead, H3K27me3-marked chromatin was enriched on day two and, even higher, on day four. In contractile cells, peripheral enrichment of H3K27me3 occurred only on day four in conjunction with and to the same extend as overall chromatin. Furthermore, patterns of H3K27 methylation closely matched that of overall chromatin in contractile cells (**Fig. 3b**), suggesting that enrichment of H3K27me3-marked chromatin mainly results from overall chromatin rearrangement in contractile cells, while enrichment of H3K27me3-marked chromatin appears to be directed in non-contractile cells as no peripheral accumulation of overall chromatin was observed here. This data validated the contrary roles of H3K9 and H3K27 methylation in cardiac development, as contractile and non-contractile CPCs showed opposing patterns of enrichment over time, and indicated that trimethylation of H3K9, but not H3K27, precedes and might coordinate chromatin rearrangements during CM maturation.

CM-specific Chromatin Organization is Abrogated in Environments with Pathological Mechanical Properties in CPCs In Vitro and Mature CMs In Vivo

To further investigate whether H3K9me3-associated chromatin reorganization is related to CM differentiation *in vitro*, we analyzed peripheral chromatin enrichment in contractile CPCs plated on either soft (13 kPa) PDMS, stiff (140 kPa) PDMS, or TCP (tissue culture plastic, >GPa). Surprisingly, on day two, CPCs plated on TCP showed a higher overall chromatin enrichment at the nuclear periphery compared to cells on either PDMS substrate (**Fig. 4a-c**). However, on day four peripheral enrichment on stiff substrates declined and cells on soft PDMS showed a higher peripheral accumulation of overall chromatin compared to both stiff PDMS and TCP. In accordance, H3K9me3-marked chromatin was equally enriched for CPCs on any substrate on day two, whereas on day four enrichment was higher on soft PDMS compared to

both stiffer substrates and was higher for stiff PDMS compared to TCP. Albeit no difference in enrichment, CPCs on soft PDMS showed higher H3K9me3 intensities at any distance compared to cells on stiffer substrates (**Fig. 4b**) in accordance with decreased expression of H3K9 methylating genes observed on stiff PDMS (**Fig. 2c**). H3K27me3-marked chromatin was slightly more enriched for CPCs on stiff PDMS on day two compared to cells on soft PDMS. After four days, enrichment of H3K27me-modified chromatin was declined on stiff substrates; however, while cells on soft substrates showed a similar enrichment of overall and H3K27me-modified chromatin, enrichment of H3K27me-modified chromatin remained higher on stiff substrates compared to overall chromatin and higher than H3K9me3-marked chromatin for cells on TCP. Furthermore, substrate stiffness only minorly affected chromatin organization in non-contractile CPCs with peripheral enrichment being low for overall and H3K9me3-marked chromatin and high for H3K27me3-modified chromatin throughout the four-day culture period (**Supplementary Fig. 2**), which overall confirmed that directed enrichment (independent of overall chromatin enrichment) of H3K27me3-marked chromatin acts in opposition to H3K9me3-marked chromatin and inhibits CM differentiation.

Hypertrophy leads to an increase in cardiac stiffness and CM dedifferentiation [3,4]. To validate our findings *in vivo*, we analyzed CM nuclei in mice that received angiotensin II (AngII) for 28 days, or saline as control, to induce hypertrophy. Reduction in ejection fraction and fractional shortening during the treatment period confirmed cardiac performance decline in mice receiving AngII, but not saline (**Fig. 4d**). CM nuclei of hypertrophic mice showed reduced enrichment of overall (DAPI), H3K27me3 and H3K9me3-marked chromatin (**Fig. 4e-g**) similar to CPC nuclei cultured on stiff substrates *in vitro*. Together these results support a direct link between cardiac differentiation and H3K9me3-associated chromatin organization and suggest

that mechanical environments can influence the establishment and retention of the nuclear architecture in CMs.

H3K9 Methylated Chromatin Domains are Localized to Intranuclear Subregions with Elevated Tensile Strains During CPC Contractions

Expression of fluorescently tagged α-actinin-2 revealed that CPC contractility was abrogated on stiff (140 kPa) PDMS compared to soft (13 kPa) PDMS substrates as overall sarcomere (S) shortening, A-band (A) shortening and Z-disk (Z) expansion were reduced more than half (-0.171 vs. -0.077 μm, -0.185 vs. -0.060 μm, 0.015 vs. -0.032 μm; **Fig. 5a-c**). In accordance, analysis of nuclear deformation recorded during CPC contraction showed that bulk linear strain and translational movement were reduced in cells plated on stiff PDMS and TCP (**Fig. 5d**).

To further investigate the role of nuclear mechanotransduction in chromatin organization, we utilized a method developed in our laboratory, termed *deformation microscopy* [25], that generates high resolution spatial strain maps from an undeformed template and a deformed target image (**Fig. 5e**). Image stacks of nuclear deformation were acquired during CPCs contraction and nuclear strain maps were calculated using frames during resting state as templates and frames during peak contraction as targets. To register patterns of epigenetic markers and intranuclear strains, cells were stained after live imaging and the common H2b-GFP channel was used to match intranuclear strain maps with chromatin marker maps to calculate strain values for nuclear regions that were predominantly occupied by chromatin associated with one of the markers or no marker (unassigned). Since both epigenetic markers, H3K27me3 and H3K9me3, are associated with forming silenced heterochromatin, we stained for serine-2 phosphorylated

RNA-polymerase II to analyze strain occupancy of actively transcribed chromatin regions in comparison [26].

H3K9me3-marked chromatin areas experienced significantly higher absolute hydrostatic strain magnitudes ($p=0.012$), but not shear or deviatoric strains ($p>0.304$), compared to average nuclear strains (**Fig. 5f**). Interestingly, subdividing hydrostatic strain values into tensile (positive) and compressive (negative) revealed that this trend arose from tensile strains alone as no significant difference could be observed for compressive hydrostatic strains between any of the investigated chromatin features ($p>0.177$). In contrast, active chromatin regions showed significantly lower absolute hydrostatic strain ($p=0.020$), a trend that was again augmented for tensile hydrostatic strain ($p=0.0003$), while no significant difference was observed for H3K27me3 areas for any of the strains investigated ($p>0.177$). Linear regression analysis of chromatin marker intensities over intranuclear strains further showed the highest degree of correlation ($R^2=0.923$) and the highest slope between all marker-strain pairs (**Fig. 5g and Supplementary Fig. 3a**). One explanation for the observed relation between H3K9me3-marked chromatin and tensile hydrostatic strain could be that nuclear strains are highest at the border and simply coincide with peripheral H3K9me3 accumulation. However, analysis of intranuclear strains over the radial distance from the nucleus center showed that strains generally declined towards the nuclear border (**Supplementary Fig. 3b**). Furthermore, analysis of preferential (angular) directionality of chromatin markers, with respect to the nuclear center, showed that H3K9me3 localization peaked within ±30° in the direction of nuclear translation only in nuclei with a tensile loading mode (**Supplementary Fig. 4**). In contrast, nuclei that showed shortening of the major axis during contraction showed diminished H3K9me3 occupancy at the angle of

nuclear translation. Overall, this data indicated that H3K9me3-marked chromatin was associated with tensile hydrostatic intranuclear strains during CPC contractions.

LINC Complex Disruption Abrogates Strain-Sensitive Relocation of H3K9 Methylated Chromatin, but Not Regulation of Histone (De)Methylases

The correlation of H3K9me3-marked chromatin areas with tensile hydrostatic strains suggested the involvement of the contractile apparatus in CMs. Co-staining of actin and H3K9me3 in CPCs revealed that sarcomere Z-disks often coincided with H3K9me3-rich chromatin clusters (**Fig. 6a**). Further analysis of CPC nuclei during contractions showed that dense, H3K9me3-rich heterochromatin clusters had higher translational movement compared to the overall nucleus (**Fig. 6b**), suggesting that H3K9me3-rich chromatin were connected to sarcomere fibers via Z-disks.

Z-disks are connected to the nucleus via LINC complexes [27], which have been shown to be crucial in nuclear mechanotransduction [6]. To directly study the role of LINC complexes in epigenetic regulation and chromatin reorganization, we analyzed nuclear maturation in CPCs after LINC disruption by overexpressing a truncated nesprin-3 protein containing the transmembrane and Kash domain (Δsyne-K3) but lacked cytoskeleton binding domains (**Fig. 6c**) [28–30]. A control vector expressed a similar truncated nesprin protein (Δsyne-CTL), which lacked the Kash domain needed for LINC complex integration. Both vectors also expressed fluorescently tagged α-actinin-2 (A2R3) to identify infected cells. CPCs that showed successful integration of Δsyne-K3 at the nuclear border after 24 hours had disorganized sarcomere fibers, particularly around the nucleus, diminished localization of nesprin-1 at the nuclear periphery (**Fig. 6d, Supplementary Fig. 5a and 5c**), and decreased nuclear bulk linear strain and translational movement during contraction (**Supplementary Fig. 5b**), all of which confirmed

nuclear decoupling. Enrichment towards the nuclear border was significantly impaired for overall (H2b) and H3K9me3-modified chromatin in decoupled cells compared to control cells, while H3K27me3 showed no distinct difference in enrichment (**Fig. 6e-g and Supplementary Fig. 5a**). Notably, overall H3K9me3 intensity was similar between decoupled and control cells, whereas H3K27me3 intensity was elevated after decoupling (**Fig. 6f**). PCR analysis revealed that gene expression of H3K9 and H3K27 histone (de)methylases was largely unchanged in decoupled cells, except for the downregulation of H3K27 demethylase *Kdm6a* (**Fig. 6h**), suggesting that nuclear mechanosensation does not regulate the expression of epigenetic mediators. Expression in non-infected control cells (NIC) was altered compared to infected control cells, indicating that adenovirus transfection affected the expression of epigenetic enzymes as previously reported [31].

In addition to epigenetic modifiers, decoupling also did not affect the expression of cardiac-specific transcription factors while structural cardiac markers were partially downregulated. Pathway analysis of global gene expression changes between CPCs plated on stiff or soft PDMS identified several signal transduction pathways involved in cell differentiation and cardiac signaling (**Supplementary Table 2**). MAPK, an important pathway for cardiac development and disease [32], and epigenetic regulation [33], was associated with pathways related to cell-ECM interactions (**Supplementary Fig. 6a**). Of those, p130Cas-mediated Rap1 signaling was of particular interest; p130Cas is a mechanosensitive focal adhesion protein [34] found within the sarcomeric Z-disks in CMs [35], making it a suitable candidate to sense substrate stiffness. In addition, p130Cas knockout mice die *in utero* due to abnormal heart growth, further linking p130Cas to cardiac development [36]. Since Z-disk extension was abrogated (**Fig. 5a-c**), we performed further analysis and confirmed that stretch-induced tyrosine 410 [37] phosphorylation of

p130Cas was reduced in CPCs plated on stiff compared to soft PDMS (**Supplementary Fig. 6b**). Together these results showed that LINC decoupling disrupted rearrangement of H3K9me3-modified chromatin during cardiac maturation but did not affect expression of cell-fate mediators such as transcription factors or epigenetic enzymes.

DISCUSSION

In this study we showed that CMs establish a distinct nuclear architecture during maturation that is characterized by a disproportional amount of chromatin at the nuclear border. Our data suggests that tensile nuclear strains during cell contractions guide the rearrangement of H3K9me3-modifieid chromatin to the nuclear periphery. Degenerative (stiff) environments, which inhibited contraction and decreased nuclear deformation, profoundly disturbed the establishment of this architecture in embryonic stages or its maintenance in adults (**Supplementary Fig. 7**). During development, stiff environments also promoted the rearrangement of H3K27me3-marked chromatin, instead of H3K9me3, which was associated with the formation of a non-contractile fibroblast-like cell-type. Our findings further support a direct link between nuclear architecture and cell differentiation, and show how environmental cues can influence cell fate by affecting chromatin organization through epigenetic regulation and nuclear mechanotransduction pathways. Taken together, our results build a new framework for the complex interactions of the exposome, epigenome and transcriptome to facilitate reliable and robust cell differentiation (**Fig. 7**). We expect that this study provides valuable insight into how degenerative conditions are related to changes in cellular microenvironments and how to direct cellular lineage commitment for new therapeutic approaches in regenerative medicine.

Potential Roles of Chromatin Organization in CMs

The observed reorganization of H3K9me3-marked chromatin during CM differentiation (and chromatin organization in general) might function to stabilize differential gene expression by segregating repressed non-cardiac genes to areas of low activity, like the nuclear envelope [38], to prevent accidental reactivation. In this study, RNAseq and PCR gene expression analysis revealed that H3K9 methylases *Ehmt1*, *Ehmt2*, *Setdb1* and *Eed* were particularly downregulated on degenerative (stiff) substrates. Recent studies have also showed that the expression of *Ehmt1/2* was decreased in the heart of hypertrophic rats and that the reactivation of cardiac fetal genes such as *Myh7*, *Nppa* and *Nppb* was associated with the loss of H3K9 methylations at those genes [3]. Furthermore, inhibition of *Ehmt1/2* was sufficient to induce hypertrophy while stabilization of *Ehmt1/2* expression counteracted effects of hypertrophy. Similarly, targeted deletion of H3K9 demethylase *Kdm4a* in the heart led to attenuated hypotrophy in mice [4]. Here we observed that H3K9me3-marked chromatin relocated back towards the nuclear center in mature CMs of hypertrophic mice, supporting the hypothesis that peripheral segregation of chromatin stabilizes its suppression. Interestingly, mechanical decoupling of CM nuclei through LINC complex disruption (on soft substrates) only minorly affected the expression of H3K9 (de)methylating enzymes or cardiac transcription factors. It is likely that cardiomyocytes integrate mechanical signals from different pathways to achieve reliable and robust cell differentiation (**Fig. 7**). RNAseq and Western Blot analysis in this study suggested that other mechanosensors, such as p130Cas located within the sarcomeric Z-disk, regulate the expression of epigenetic mediators via Rap1 and MAPK signaling (**Supplementary Fig. 6**).

In addition to stabilizing cardiac gene transcription, the CM nuclear architecture might also have a structural function as has been reported for other types of cells [13,14,39]. The high ratio of peripheral heterochromatin might play a protective role as heterochromatin has been shown to

increase nuclear rigidity independent of lamins [40]. Chromatin void cavities could provide a protective environment for gene transcription in cells that are mostly not replaced throughout their lifetime and that must endure high and constant cyclic mechanical stresses. This is supported by our observation that nuclear areas of actively transcribed chromatin experience lower (tensile) hydrostatic strains and that prolific, non-contractile cardiac fibroblasts showed a homogeneous chromatin organization.

Potential Role of Nuclear Mechanosensation in CMs

The role of nuclear mechanotransduction has long been debated. While it has been shown that LINC complexes are involved in mechanosensitive gene regulation [41], no distinct mechanism has been reported so far. We provided evidence that nuclear strains during cell contractions, transferred from the sarcomeric Z-disks via LINC complexes, guide the reorganization of H3K9me3-modified chromatin in CMs during development. In contrast, the formation of a non-contractile fibroblast-like cell-type was associated with the reorganization of H3K27me3-marked chromatin instead. We argue therefore, that CMs use nuclear strains as an additional feedback for differentiation by consolidating the suppression of H3K9me3-marked non-cardiac genes through peripheral segregation as described above. This mechanism would be beneficial during development as it ensures that only CMs with high contractility mature, while others become fibroblasts or undergo apoptosis. Neurons are known to use a similar activity-based mechanism during development [42]. Further investigation will show whether this nuclear-feedback is used by other load-bearing cells as well.

Potential Mechanisms of Mechanosensitive Chromatin Reorganization

How nuclear strains could guide chromatin rearrangement is unclear, but it is likely to involve nuclear motor proteins. For example, nuclear myosin 1 (NM1) has been shown to be

necessary for chromatin relocation in response to serum activation [43] and DNA damage [44]. Nuclear motor proteins, other than NM1, are poorly characterized, however, and more research is needed to understand their role and activation in the nucleus. After transport, nuclear envelope transmembrane proteins (NET) could anchor chromatin to the nuclear envelope. NETs have been shown to be tissue specific and might also recognize epigenetic modification of chromatin [10,45,46].

The strict association of H3K9me3 with tensile, but not compressive, hydrostatic strains indicated the involvement of stretch-activation. It has been argued that LINC complexes are the nuclear analog to stretch-sensitive focal-adhesions at the cell membrane [5] and research on isolated nuclei has shown that LINC complexes are necessary for stretch-induced nuclear mechanotransduction [6]. Similarly, we found in this study that LINC complex seem to be important for stretch-induced chromatin reorganization in CMs. Direct evidence for stretch-sensitivity of LINC complex components (nesprins and SUNs) is lacking, however, and it remains to be seen whether LINC complex or associated proteins (*e.g.* lamins) bear inherent mechanosensitivity. Stretch-activation could ultimately control motor-protein activity and/or the recruitment of NETs (**Fig. 7**) to control chromatin reorganization using mechanisms similar to focal adhesions.

METHODS

Substrate Fabrication

To mimic mechanical environments of mature and pathological stiffened cardiac tissue [19,20,47], cell culture dishes were coated with soft or stiff PDMS (Sylgard®527, Dow Corning) by using different mixing ratios (base:curing agent): 1:1 (E=12.7 ± 5.0 kPa) and 1:4 (E=139.7 ± 16.2 kPa). To enable live imaging at high magnification using a 100× objective, PDMS was

deposited as thin layer (~100 μm) in gridded imaging dishes (μ-Dish 35 mm high Grid-500, ibidi). PDMS coated dishes were degassed under vacuum for 30 min, cured for 1h at 80°C, ozone-activated via corona arc-discharge (~30s) and coated with Reduced Growth Factor Basement Membrane Matrix (Geltrex®, ThermoFisher) for 1h at 37°C to provide complex attachment sides similar to the cardiac basement membrane. PDMS stiffness was determined via AFM using a spherical borosilicate glass tip (diameter=10 μm, stiffness=0.85 N/m), and Young's modulus *E* was calculated using a Hertz contact model[48].

Cardiac Precursor Cell Isolation and Culture

B6.Cg-Tg (HIST1H2BB/EGFP) 1Pa/J mice (Stock No: 006069) were obtained from Jackson Laboratory. All animal procedures were performed following Institutional Animal Care & Use Committee approval. Embryonic mice hearts were harvested 18.5 days post conception. Hearts were minced and incubated in a digestive mix for 30 min at 37°C. Digestive mix contained 2 mg/ml Papain (Sigma), 500 μg/ml Liberase TM (Roche), 5 mM L-Cysteine (Sigma) and 10 μg/ml DNase-I (Sigma). CPCs were isolated by gently pipetting digested hearts up and down using a 1 ml pipette and cells were cultured on prepared substrates in DMEM F12 Advanced (Life Technologies) containing 10% fetal bovine serum, 1% penicillin-streptomycin (Life Technologies) and 25 mM HEPES (Life Technologies) at a density of 50,000 cells/cm^2. Samples were incubated at 37°C and 5% CO_2. CPCs started spontaneous contractions within 24h of plating.

Immunofluorescence Staining

Cells were fixed in 4% ice-cold PFA for 10min, permeabilized with 1% Triton-X100 in PBS for 15 min and blocked with 10%NGS, 1% BSA in 0.1% PBT (0.1% Tween-20 in PBS) for 60 min. Primary incubation was performed at 4°C overnight in 0.1% PBT containing 1% BSA.

Secondary incubation was performed in primary incubation buffer for 45 min (RT) at a dilution of 1:500. Actin was counterstained with Texas Red-X Phalloidin (Life Technologies). Primary antibodies: H3K9me3 (abcam, ab8898, 1:800), H3K27me3 (abcam, ab6002, 1:200), RNA polymerase II CTD repeat YSPTSPS phospho S2 (abcam, ab24758, 1:400) and nesprin-1 (abcam, ab24742, 1:500).

Tissue Sectioning and Staining

After harvest, tissues were washed in PBS and fixed in 4% PFA at 4°C overnight. Tissue were then washed again in PBS, embedded in 6% agarose and sectioned into 100 μm thin slices using a vibratome (VT1000 S, Leica). Tissue sections were further immunostained as described above.

Analysis of Chromatin Markers Occupancy

Image stacks of immunostained nuclei were recorded on a Nikon A1R confocal microscope using a 60× oil immersion objective. A custom MATLAB code was used to calculate the intensity of each chromatin marker with respect to distance of the nuclear border. Briefly, the H2b-eGFP image stack was used to determine the nuclear border and the nuclear center for each nucleus. For each pixel, the distance to the nuclear center was calculated and image intensities for each marker channel were collected. Nuclear center distances were normalized to the maximum distance of each corresponding center trajectory resulting in a normalized center distance of 0 for the center 1 for the nuclear periphery. Normalized nuclear center distances were then binned in 0.01 steps (100 bins total) and marker intensities for pixels in the same bin were averaged.

For angular analysis, the angle of each pixel with respect to the nuclear center was obtained with the nuclear translation angle set as 0° (**Supplementary Fig. 4b**). Nuclear

translation angle was determined as the angle of the trajectory that connected the nuclear centers before (resting) and during CPC contraction. Pixels were binned in 1° steps and marker intensities for each channel were averaged for each bin. SEM indicates deviations only between cells not the deviation within single cells for both distance and angular analysis.

Generation of Intranuclear Strain Maps

After 2 days of culture on soft PDMS, image stacks were captured using an inverted epi-fluorescence microscope (Nikon Ti-Eclipse) with a 100× oil immersion objective and an EMCCD camera (iXon^{EM}+, Andor). Stacks were captured at 6.4 fps over a period of 10 s, during which photobleaching was negligible. For each nucleus, one contraction cycle was selected from the image stack to perform nuclear deformation analysis using *deformation microscop*y developed previously [25,49].

Adenovirus Generation and Transduction

Adenoviral vectors for LINC disruption experiments were generated as described before [50] using the AdEasy vector system. The decoupling and control construct were assembled via Gibson cloning using NEBuilder® HiFi DNA Assembly Master Mix (NEB). The decoupling construct contained the C-terminal end of the nesprin-3 gene (*Syne3*) including the transmembrane (Tm) and the KASH domain. The N-terminus was replaced by a far-red fluorescence protein (mNeptune2.5) for visualization and a signal peptide (SP, from *Tor1a*) for membrane integration. The control construct was identical to the decoupling construct but lacked the KASH domain. AdEasy plasmids were a gift from Leslie Leinwand. pcDNA3-mNeptune2.5 and pcDNA3-mRuby2 were a gift from Michael Lin (Addgene, #51310 and #40260) [51]. For chromatin marker analysis in decoupled CPCs, cells were infected at day one with 10×MOI, as

determined by plaque assay, and fixed and stained for H3K9me3 or H3K27me3 at day 2 of culture.

Hypertrophic Animal Model

Female C57BL/6J mice (Jackson Laboratory) were surgically implanted with a mini-osmotic pump (ALZET Model 2004, DURECT Corporation) to deliver either saline (n=5) or AngII (n=4) at a rate of 0.28 μL/hr for 28 days. For the AngII group, the AngII powder was dissolved in saline to provide a 1000 ng/kg/min infusion rate. Mice were monitored at baseline and again on day 28 post-surgery using a high resolution, small animal ultrasound imaging system (Vevo2100 Imaging System, FUJIFILM VisualSonics) to assess cardiac size and function [52]. After 28 days, mice were euthanized, hearts harvested, and the left ventricles were cut along the transverse plane. Tissue sectioning and staining was performed as described above. All animal procedures were approved by the Institutional Animal Care and Use Committee.

Small Animal Ultrasound Imaging

A high resolution, small animal *in vivo* ultrasound imaging system was used to assess cardiac size and function at baseline and again on day 28 post-surgery. Briefly, anesthetized mice (1-3% isoflurane) were positioned supine on a heated stage. Body temperature was monitored using a rectal probe, while cardiac and respiratory rates were monitored using stage electrodes. Hair on the thoracic region was removed with depilatory cream and ultrasound gel was applied. A linear array transducer (MS550D) was used to view both the long and short axes of the heart. Two-dimensional cine loops in brightness mode (B-mode) and motion mode (M-mode) were collected. In addition, high temporal resolution cine loops were acquired using ECG-gated Kilohertz Visualization (EKV). These images were analyzed with Vevo2100 software (FUJIFILM VisualSonics) to determine ejection fraction and fractional shortening.

Gene Expression Analysis

Total RNA was extracted from CPCs after 4 days in culture on either soft or stiff PDMS or TCP (n=4) using the AurumTM Total RNA Mini Kit. RNA was reverse transcribed into cDNA via iScriptTM Reverse Transcription Supermix and real-time quantitative PCR was performed with SsoAdvancedTM Universal SYBR® Green Supermix in a CFX96 Touch™ thermocycler (all kits and devices from Bio-Rad Laboratories) using 10 ng of cDNA as input. Primers were custom designed using NCBI primer blast, cross-confirmed in Ensembl gene database and synthesized by IdtDNA. Primers span at least one exon-exon junction. Relative expression change was calculated using the ΔΔCt method. All data was normalized to the reference genes *Gapdh* and *ActB* as established in previous heart failure studies [53,54]. Primer sequences are listed in **Supplementary Table 3**.

RNAseq

Total RNA was extracted from CPCs after 4 days in culture on either soft or stiff PDMS (n=4) using the AurumTM Total RNA Mini Kit. Libraries were constructed by the Purdue Genomics Core Facilities according to standard protocols using TruSeq Stranded mRNA Library Prep Kit (Illumina). Samples were run on a HiSeq 2500 (Illumina) with 200 bp paired-end reads. The filtered Illumina reads were pre-processed and mapped by the Purdue Bioinformatics Core. Sequence quality was assessed using FastQC (v0.11.2) for all samples and quality trimming was done using FASTX toolkit (v0.0.13.2) to remove bases with less than Phred33 score of 30 and resulting reads of at least 50 bases were retained. The quality trimmed reads were mapped against the bowtie2-indexed reference genome downloaded from Ensembl using Tophat (v2.0.14) with default parameters.

Genes associated with the GO term *histone modification* (GO:0016570) were obtained from AmiGO 2 (*http://amigo.geneontology.org/amigo*) and differentially expressed genes ($p<0.2$) in this ontology were used to screen for child GO terms using AmiGO's term enrichment tool (v1.8). Pathways with enriched differential gene expression were screened using the KEGG database via the functional annotation tool DAVID (*https://david.ncifcrf.gov/*). Analyses of functionally grouped networks was performed using the ClueGO (v2.5.0) app on the Cytoscape (v3.6.0) software tool.

Western Blot Analysis

CPCs cultured on soft or stiff PDMS substrates for four days were lysed in tris-triton buffer containing a protease/phosphatase inhibitor mix (Sigma). Protein concentrations were determined using Bradford Assay Kit 1 (Bio-Rad) and 30µg of protein were loaded onto 8% SDS-Page Gels (Thermo Scientific), transferred to PVDF membranes (EMD Millipore) and immunodetected using an ECL substrate kit (Life Technologies) and a PXi imaging system (Syngene). Densitometric quantification was performed using ImageJ (NIH). Primary antibodies: p130Cas (cell signaling, #13846), phospho-p130Cas Tyr410 (cell signaling, #4011) and Gapdh (cell signaling, #5174).

Sarcomere Shortening Analysis

CPCs cultured on soft or stiff PDMS were infected with adenovirus carrying the decoupling control vector (CTL) on day two of culture and image stacks of mRyub2-tagged α-actinin2 were acquired during CPC contractions on day three. A custom written MATLAB code was used to quantify the length of different sarcomere features before and during contraction from α-actinin2 fluorescence intensity profiles stretching 15-20µm and containing 8-12 α-actinin2-rich Z-disks (**Fig. 6d, e**). Overall sarcomere lengths were determined as the distance

between neighboring peaks. Data points between peaks were interpolated (cubic) and the mid-intensity between maximum (peak) and minimum (valley) was used to separate the Z-disks from A-bands for each segment (**Fig. 6e, bottom**). Values along one intensity profile were averaged and the difference in length before and during contraction for each sarcomere feature were calculated. A total of 25 intensity profiles of different sarcomere fibers were analyzed for each substrate, respectively.

Statistical Analysis

One-way ANOVA or two-tailed T-test analysis was performed to evaluate statistical significance using JMP Pro12 software (SAS Institute). Displayed error (SD=standard deviation, SEM=standard error of the mean), sample numbers, significances and statistical test that was used are indicated in the figure captions.

ACKNOWLEDGEMENTS

We are grateful to Leslie Leinwand and Stephen J. Langer for providing materials and technical assistance for the generation of adenoviruses. We also thank Michael Rafuse for technical assistance regarding tissue sectioning. This work was supported in part by NIH grants R01 AR063712 and R21 AR066230, and NSF grant CMMI CAREER 1349735.

AUTHOR CONTRIBUTIONS

Conceptualization, B.S., S.G., C.J.G., S.C., and C.P.N.; Methodology, B.S., S.G., C.J.G., S.C., and C.P.N.; Software, B.S. and S.G.; Formal Analysis, B.S. and S.G.; Investigation, B.S., A.G.B and S.E.S.; Writing – Original Draft, B.S.; Writing – Review & Editing, All authors; Funding Acquisition, C.P.N.; Resources, C.J.G. and C.P.N.; Supervision, S.G., S.C., and C.P.N.

DECLARATION OF INTERESTS

The authors declare no competing interests.

REFERENCES

1. Swift, J. *et al.* The nuclear lamina is mechano-responsive to ECM elasticity in mature tissue. *J. Cell Sci.* **127,** 3005–15 (2014).
2. Engler, A. J., Sen, S., Sweeney, H. L. & Discher, D. E. Matrix elasticity directs stem cell lineage specification. *Cell* **126,** 677–89 (2006).
3. Thienpont, B. *et al.* The H3K9 dimethyltransferases EHMT1/2 protect against pathological cardiac hypertrophy. *J. Clin. Invest.* **127,** 335–348 (2017).
4. Zhang, Q. J. *et al.* The histone trimethyllysine demethylase JMJD2A promotes cardiac hypertrophy in response to hypertrophic stimuli in mice. *J. Clin. Invest.* **121,** 2447–2456 (2011).
5. Aureille, J., Belaadi, N. & Guilluy, C. Mechanotransduction via the nuclear envelope: a distant reflection of the cell surface. *Curr. Opin. Cell Biol.* **44,** 59–67 (2017).
6. Guilluy, C. *et al.* Isolated nuclei adapt to force and reveal a mechanotransduction pathway in the nucleus. *Nat. Cell Biol.* **16,** 376–381 (2014).
7. Taranum, S. *et al.* LINC complex alterations in DMD and EDMD/CMT fibroblasts. *Eur. J. Cell Biol.* **91,** 614–628 (2012).
8. Banerjee, I. *et al.* Targeted ablation of nesprin 1 and nesprin 2 from murine myocardium results in cardiomyopathy, altered nuclear morphology and inhibition of the biomechanical gene response. *PLoS Genet.* **10,** e1004114 (2014).

9. Solovei, I. *et al.* LBR and lamin A/C sequentially tether peripheral heterochromatin and inversely regulate differentiation. *Cell* **152,** 584–98 (2013).

10. de Las Heras, J. I. *et al.* Tissue specificity in the nuclear envelope supports its functional complexity. *Nucleus* **4,** 460–77 (2014).

11. Joffe, B., Leonhardt, H. & Solovei, I. Differentiation and large scale spatial organization of the genome. *Curr. Opin. Genet. Dev.* **20,** 562–9 (2010).

12. Parada, L. A., McQueen, P. G. & Misteli, T. Tissue-specific spatial organization of genomes. *Genome Biol.* **5,** R44 (2004).

13. Pombo, A. & Dillon, N. Three-dimensional genome architecture: players and mechanisms. *Nat. Rev. Mol. Cell Biol.* **16,** 245–57 (2015).

14. Olins, A. L. & Olins, D. E. Cytoskeletal influences on nuclear shape in granulocytic HL-60 cells. *BMC Cell Biol.* **5,** 30 (2004).

15. Kim, S. H. *et al.* Spatial genome organization during T-cell differentiation. *Cytogenet. Genome Res.* **105,** 292–301 (2004).

16. Solovei, I. *et al.* Nuclear architecture of rod photoreceptor cells adapts to vision in mammalian evolution. *Cell* **137,** 356–68 (2009).

17. Hogan, M. S., Parfitt, D. E., Zepeda-Mendoza, C. J., Shen, M. M. & Spector, D. L. Transient pairing of homologous Oct4 alleles accompanies the onset of embryonic stem cell differentiation. *Cell Stem Cell* **16,** 275–288 (2015).

18. Barnes, J. M., Przybyla, L. & Weaver, V. M. Tissue mechanics regulate brain development, homeostasis and disease. *J. Cell Sci.* **130,** 71–82 (2017).

19. Engler, A. J. *et al.* Myotubes differentiate optimally on substrates with tissue-like stiffness: Pathological implications for soft or stiff microenvironments. *J. Cell Biol.* **166,**

877–887 (2004).

20. Jacot, J. G., McCulloch, A. D. & Omens, J. H. Substrate stiffness affects the functional maturation of neonatal rat ventricular myocytes. *Biophys. J.* **95,** 3479–87 (2008).

21. Young, J. L., Kretchmer, K., Ondeck, M. G., Zambon, A. C. & Engler, A. J. Mechanosensitive kinases regulate stiffness-induced cardiomyocyte maturation. *Sci. Rep.* **4,** 6425 (2014).

22. Filion, G. J. *et al.* Systematic protein location mapping reveals five principal chromatin types in Drosophila cells. *Cell* **143,** 212–24 (2010).

23. Mysliwiec, M. R. *et al.* Jarid2 (Jumonji, AT rich interactive domain 2) regulates NOTCH1 expression via histone modification in the developing heart. *J. Biol. Chem.* **287,** 1235–1241 (2012).

24. Dal-Pra, S., Hodgkinson, C. P., Mirotsou, M., Kirste, I. & Dzau, V. J. Demethylation of H3K27 Is Essential for the Induction of Direct Cardiac Reprogramming by MIR Combo. *Circ. Res.* **120,** 1403–1413 (2017).

25. Ghosh, S. *et al.* Deformation microscopy for dynamic intracellular and intranuclear mapping of mechanics with high spatiotemporal resolution. *bioRxiv* 403261 (2018). doi:10.1101/403261

26. Ni, Z. *et al.* P-TEFb is critical for the maturation of RNA polymerase II into productive elongation in vivo. *Mol. Cell. Biol.* **28,** 1161–70 (2008).

27. Stroud, M. J., Banerjee, I., Veevers, J. & Chen, J. Linker of nucleoskeleton and cytoskeleton complex proteins in cardiac structure, function, and disease. *Circ. Res.* **114,** 538–48 (2014).

28. Lu, W. *et al.* Nesprin interchain associations control nuclear size. *Cell. Mol. Life Sci.* **69,**

3493–3509 (2012).

29. Grady, R. M., Starr, D. a, Ackerman, G. L., Sanes, J. R. & Han, M. Syne proteins anchor muscle nuclei at the neuromuscular junction. *Proc. Natl. Acad. Sci. U. S. A.* **102,** 4359–4364 (2005).

30. Iyer, K. V., Pulford, S., Mogilner, A. & Shivashankar, G. V. Mechanical activation of cells induces chromatin remodeling preceding MKL nuclear transport. *Biophys. J.* **103,** 1416–1428 (2012).

31. Balakrishnan, L. & Milavetz, B. Epigenetic Regulation of Viral Biological Processes. *Viruses* **9,** (2017).

32. Rose, B. A., Force, T. & Wang, Y. Mitogen-activated protein kinase signaling in the heart: angels versus demons in a heart-breaking tale. *Physiol. Rev.* **90,** 1507–46 (2010).

33. Riccio, A. Dynamic epigenetic regulation in neurons: enzymes, stimuli and signaling pathways. *Nat. Neurosci.* **13,** 1330–7 (2010).

34. Sawada, Y. *et al.* Force Sensing by Mechanical Extension of the Src Family Kinase Substrate p130Cas. *Cell* **127,** 1015–1026 (2006).

35. Kovacic-Milivojević, B., Damsky, C. C., Gardner, D. G. & Ilić, D. Requirements for the localization of p130 Cas to Z-lines in cardiac myocytes. *Cell. Mol. Biol. Lett.* **7,** 323–9 (2002).

36. Honda, H. *et al.* Cardiovascular anomaly, impaired actin bundling and resistance to Src-induced transformation in mice lacking p130(Cas). *Nat. Genet.* **19,** 361–365 (1998).

37. Akimoto, T. *et al.* Skeletal muscle adaptation in response to mechanical stress in p130cas $^{-/-}$ mice. *Am. J. Physiol. Physiol.* **304,** C541–C547 (2013).

38. Sexton, T., Schober, H., Fraser, P. & Gasser, S. M. Gene regulation through nuclear

organization. *Nat. Struct. Mol. Biol.* **14,** 1049–55 (2007).

39. Queisser, G., Wiegert, S. & Bading, H. Structural dynamics of the cell nucleus: basis for morphology modulation of nuclear calcium signaling and gene transcription. *Nucleus* **2,** 98–104 (2011).

40. Stephens, A. D. *et al.* Chromatin histone modifications and rigidity affect nuclear morphology independent of lamins. *Mol. Biol. Cell* **29,** 220–233 (2018).

41. Alam, S. G. *et al.* The mammalian LINC complex regulates genome transcriptional responses to substrate rigidity. *Sci. Rep.* **6,** 38063 (2016).

42. Spitzer, N. C. Electrical activity in early neuronal development. *Nature* **444,** 707–712 (2006).

43. Mehta, I. S., Amira, M., Harvey, A. J. & Bridger, J. M. Rapid chromosome territory relocation by nuclear motor activity in response to serum removal in primary human fibroblasts. *Genome Biol.* **11,** R5 (2010).

44. Kulashreshtha, M., Mehta, I. S., Kumar, P. & Rao, B. J. Chromosome territory relocation during DNA repair requires nuclear myosin 1 recruitment to chromatin mediated by ϒ-H2AX signaling. *Nucleic Acids Res.* **44,** 8272–91 (2016).

45. Wilkie, G. S. *et al.* Several Novel Nuclear Envelope Transmembrane Proteins Identified in Skeletal Muscle Have Cytoskeletal Associations. *Mol. Cell. Proteomics* **10,** M110.003129 (2011).

46. Zuleger, N. *et al.* Specific nuclear envelope transmembrane proteins can promote the location of chromosomes to and from the nuclear periphery. *Genome Biol.* **14,** R14 (2013).

47. Pasqualini, F. S. *et al.* Traction force microscopy of engineered cardiac tissues. *PLoS One*

13, e0194706 (2018).

48. Xu, X., Li, Z., Cai, L., Calve, S. & Neu, C. P. Mapping the Nonreciprocal Micromechanics of Individual Cells and the Surrounding Matrix Within Living Tissues. *Sci. Rep.* **6,** 24272 (2016).

49. Henderson, J. T., Shannon, G., Veress, A. I. & Neu, C. P. Direct measurement of intranuclear strain distributions and RNA synthesis in single cells embedded within native tissue. *Biophys. J.* **105,** 2252–61 (2013).

50. Pugach, E. K., Blenck, C. L., Dragavon, J. M., Langer, S. J. & Leinwand, L. A. Estrogen receptor profiling and activity in cardiac myocytes. *Mol. Cell. Endocrinol.* **431,** 62–70 (2016).

51. Chu, J. *et al.* Non-invasive intravital imaging of cellular differentiation with a bright red-excitable fluorescent protein. *Nat. Methods* **11,** 572–578 (2014).

52. Pereyra, A. S. *et al.* Loss of cardiac carnitine palmitoyltransferase 2 results in rapamycin-resistant, acetylation-independent hypertrophy. *J. Biol. Chem.* **292,** 18443–18456 (2017).

53. Li, Q. *et al.* Selection of reference genes for normalization of quantitative polymerase chain reaction data in mouse models of heart failure. *Mol. Med. Rep.* **11,** 393–9 (2015).

54. Martino, A. *et al.* Selection of reference genes for normalization of real-time PCR data in minipig heart failure model and evaluation of TNF-α mRNA expression. *J. Biotechnol.* **153,** 92–9 (2011).

FIGURES

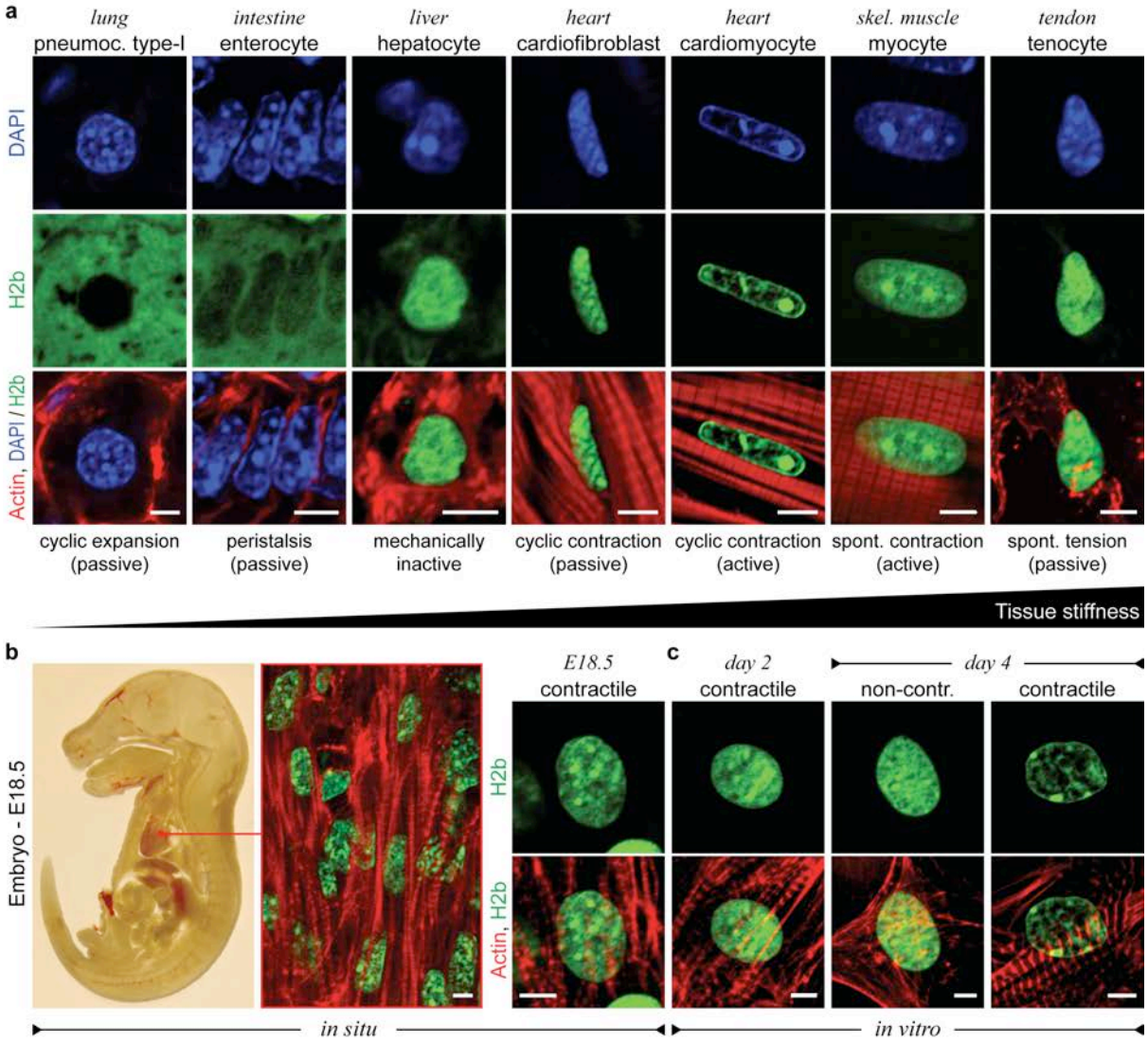

Fig. 1. Cardiomyocytes adopt a distinct nuclear architecture with high amounts of peripheral chromatin during development. a) Diverse tissues were harvested from H2b-eGFP adult mice and stained for actin. DAPI was used as DNA counterstain for soft tissues with weak H2b-eGFP fluorescence. Mature cardiomyocytes have an elongated nucleus with a high ratio of peripheral chromatin compared to other cell types. **b)** Embryos from H2b-eGFP mice were harvested at embryonic day (E)18.5, sectioned and stained for actin. Left: whole embryo mid-section. Middle: close-up of embryonic cardiac tissue from mid-section. Right: close-up of an embryonic cardiomyocyte nucleus, which shows a diffuse nuclear organization unlike mature cardiomyocytes. **c)** Cardiac precursor cells were isolated from embryonic hearts and plated on soft (13 kPa) PDMS substrates for two or four days. Cells with contractile sarcomere structures show a change in nuclear organization at day four. All scale bars=5 µm.

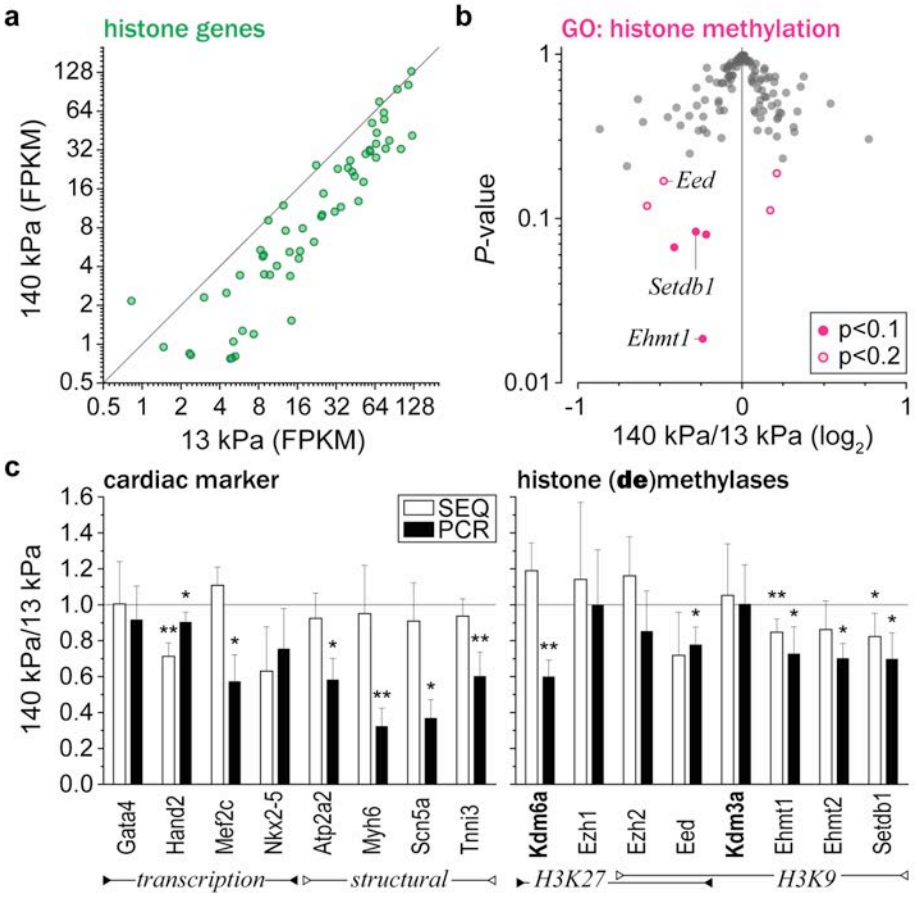

Fig. 2. Substrate stiffness affects expression of histone and histone modifying genes in CPCs. Cardiac precursor cells (CPC) were isolated from E18.5 H2b-eGFP embryo hearts and cultured on soft (13 kPa) or stiff (140 kPa) PDMS for four days after which total RNA was collected. **a)** RNAseq analysis showed that of 63 expressed histone genes most were downregulated on stiff PDMS, suggesting inhibited chromatin remodeling. n=4; FPKM: Fragments Per Kilobase of transcript per Million mapped reads. **b)** Volcano plot of genes associated with the gene ontology term *histone methylation* (GO:0016571) as determined by RNAseq. Indicated are genes coding for H3K9 methylases, which were amongst the most significantly altered (see also Supplementary Table 1). **c)** PCR validation of RNAseq (SEQ) data verified downregulation of H3K9 methylating genes and showed that cardiac transcription and structural marker were decreased on stiff substrates. H3K9 demethylase *Kdm3a* and H3K27-specific methylase *Ezh1* showed no expression change while H3K27 demethylase *Kdm6a* was downregulated, overall indicating inverse methylation activity between H3K9 and H3K27 for CPCs on stiff substrates. SD; n=4; T-Test: * $p<0.05$, ** $p<0.01$.

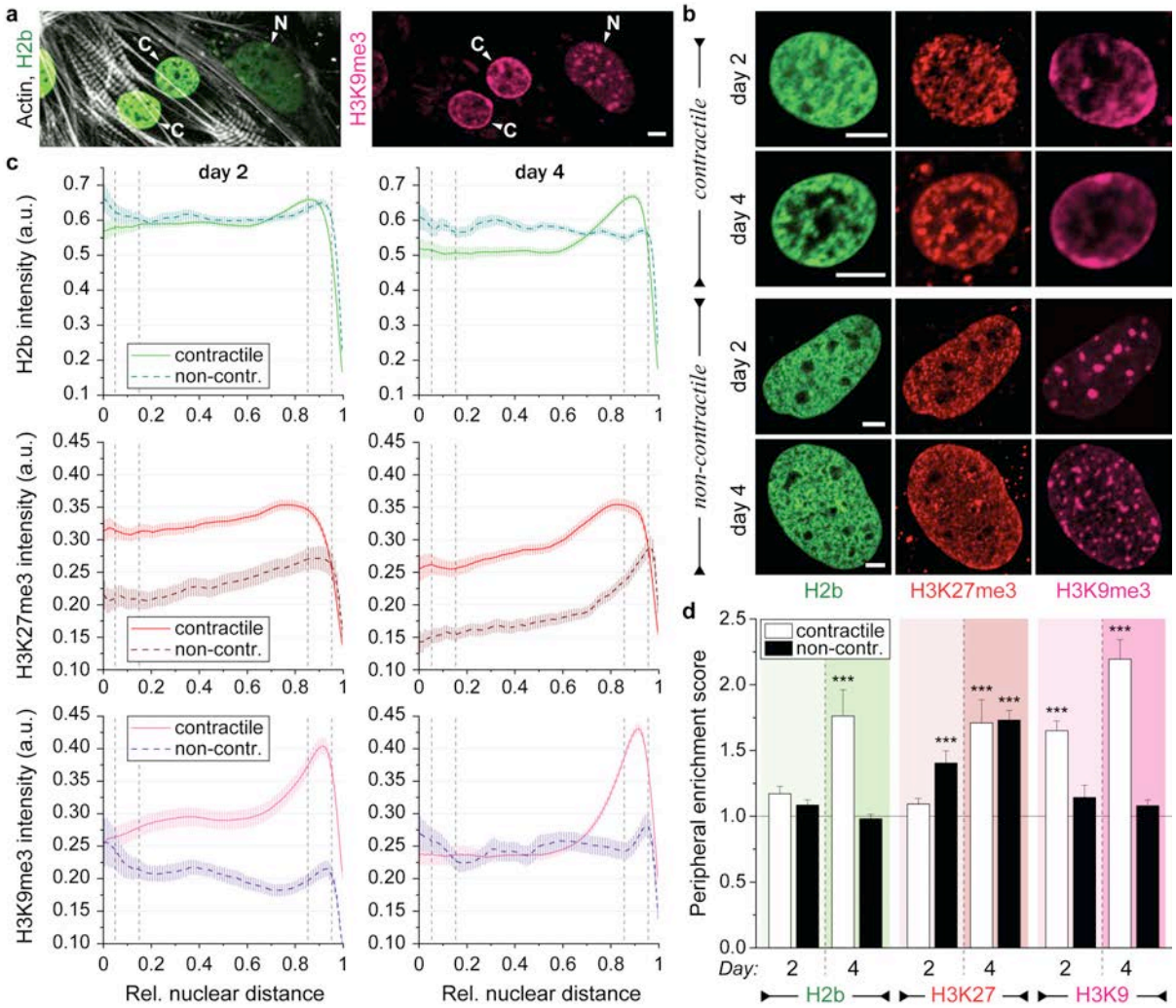

Fig. 3. Peripheral enrichment of H3K9 trimethylated chromatin precedes that of overall chromatin in contractile, but not non-contractile, cardiac precursor cells *in vitro*. Cardiac precursor cells (CPC) were isolated from E18.5 H2b-eGFP embryo hearts and cultured on soft (13 kPa) PDMS substrates. **a)** After two days in culture, contractile cells (C) that formed sarcomeres showed peripheral accumulation of H3K9me3-modified chromatin while non-contractile cells (N) that formed actin stress fibers did not. **b)** Contractile and non-contractile CPCs were stained for H3K27me3 and H3K9me3 and images of nuclei were acquired at day two or four of culture. **c)** Stained CPC nuclei were analyzed for peripheral enrichment of overall chromatin (H2b) or epigenetically marked chromatin using a custom MATLAB code. Fluorescence intensity of each chromatin channel was analyzed with respect to its relative distance to the nuclear center (0=center, 1=periphery). Black lines indicate the center bin (0.05-0.15) and peripheral bin (0.85-0.95) used to calculate enrichment scores. SEM; n>60. **d)** For each marker in each nucleus, an enrichment score was calculated as the quotient of intensity of the peripheral bin divided by the center bin. Contractile CPCs, but not non-contractile, showed a shift of overall chromatin towards the nuclear border at day four. This was preceded by an enrichment of H3K9me3-marked chromatin at day two, again only in contractile CPCs, while non-contractile cells showed enrichment of H3K27me3-modified chromatin at this time. SEM; n>60; T-test, *** $p<0.001$. All scale bars=5 µm.

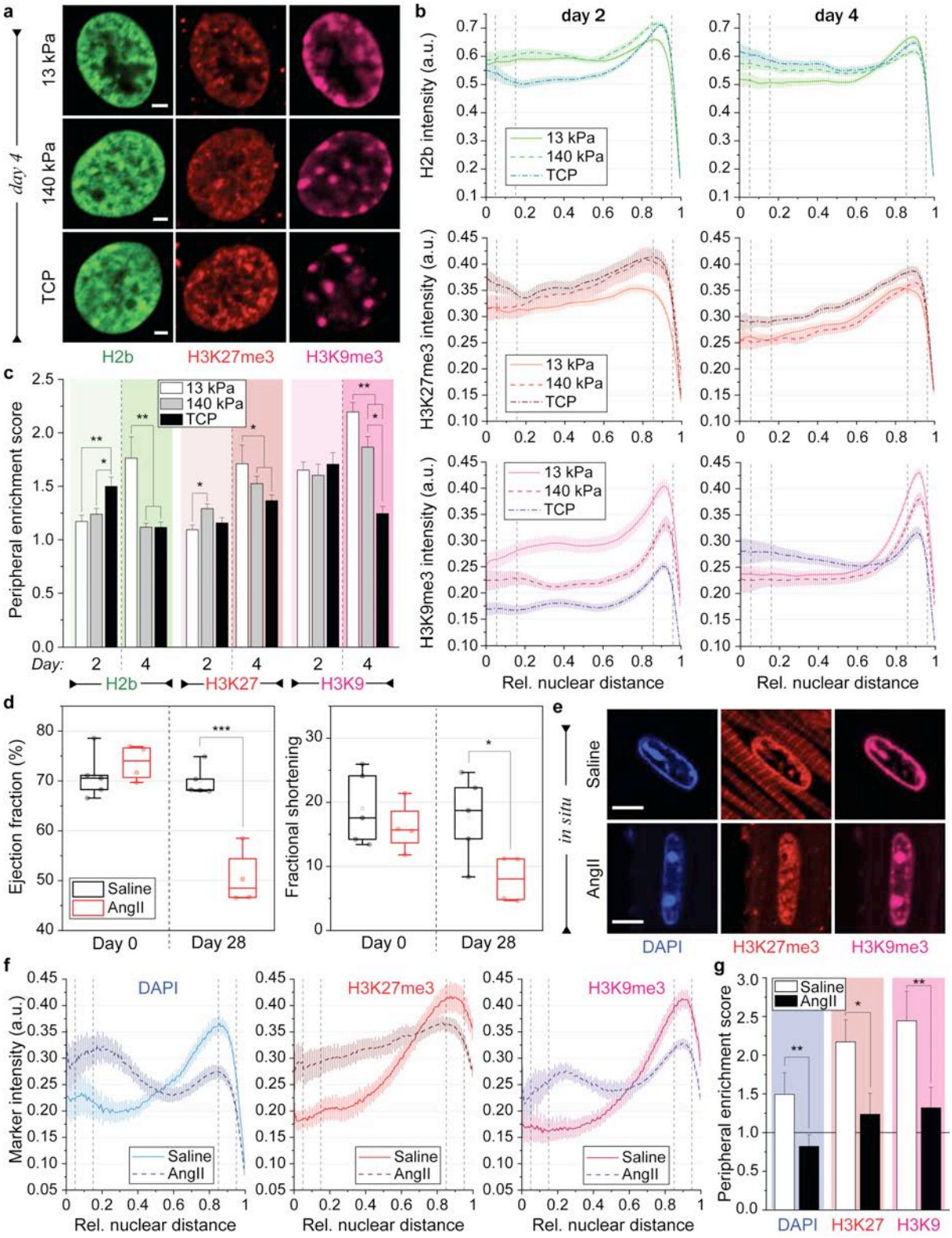

Fig. 4. CM-specific chromatin organization is abrogated in environments with pathological mechanical properties in contractile CPCs *in vitro* and mature CMs *in vivo*. a) Cardiac precursor

cells (CPC) were isolated from E18.5 H2b-eGFP embryo hearts and cultured on either soft (13 kPa) PDMS, stiff (140 kPa) PDMS or TCP for two or four days after which nuclei were stained for H3K27me3 and H3K9me3. **b)** CPC nuclei were evaluated for peripheral enrichment of overall chromatin (H2b) or epigenetically marked chromatin using a custom MATLAB code that analyzed marker intensity with respect to its relative distance to the nuclear center (0=center, 1=periphery). Black lines indicate center and peripheral bin. Error bars=SEM; $n \geq 60$. **c)** Enrichment scores for each chromatin marker were calculated as the quotient of intensity of the peripheral bin (0.85-0.95) divided by the center bin (0.05-0.15). Enrichment of overall and H3K9me3-marked chromatin was abrogated on day four in nuclei of cells plated on stiff PDMS and TCP compared to soft PDMS. SEM; $n \geq 60$; ANOVA: * $p<0.05$, ** $p<0.01$, *** $p<0.001$. **d)** Mice treated with angiotensin II (AngII, n=4), to induce hypertrophic conditions, showed reduced ejection fraction and fractional shortening after 28 days of treatment compared to day 0, while saline receiving control mice (n=5) showed no significant difference; T-test: * $p<0.05$, *** $p<0.001$. **e)** After 28 days, hearts were harvested and stained for H3K27me3 and H3K9me3. DAPI was used as DNA counterstain. **f, g)** Immunostained cardiac sections of hypertrophic (AngII) or control mice (Saline) were analyzed for peripheral enrichment of overall chromatin (DAPI) or epigenetically marked chromatin using a custom MATLAB code and enrichment scores were calculated. Enrichment of overall and methylated chromatin was abrogated in cardiac nuclei of hypertrophic mice while control mice showed a mature cardiac phenotype. SEM; $n \geq 40$; T-test: * $p<0.05$, ** $p<0.01$. All scale bars=5 µm.

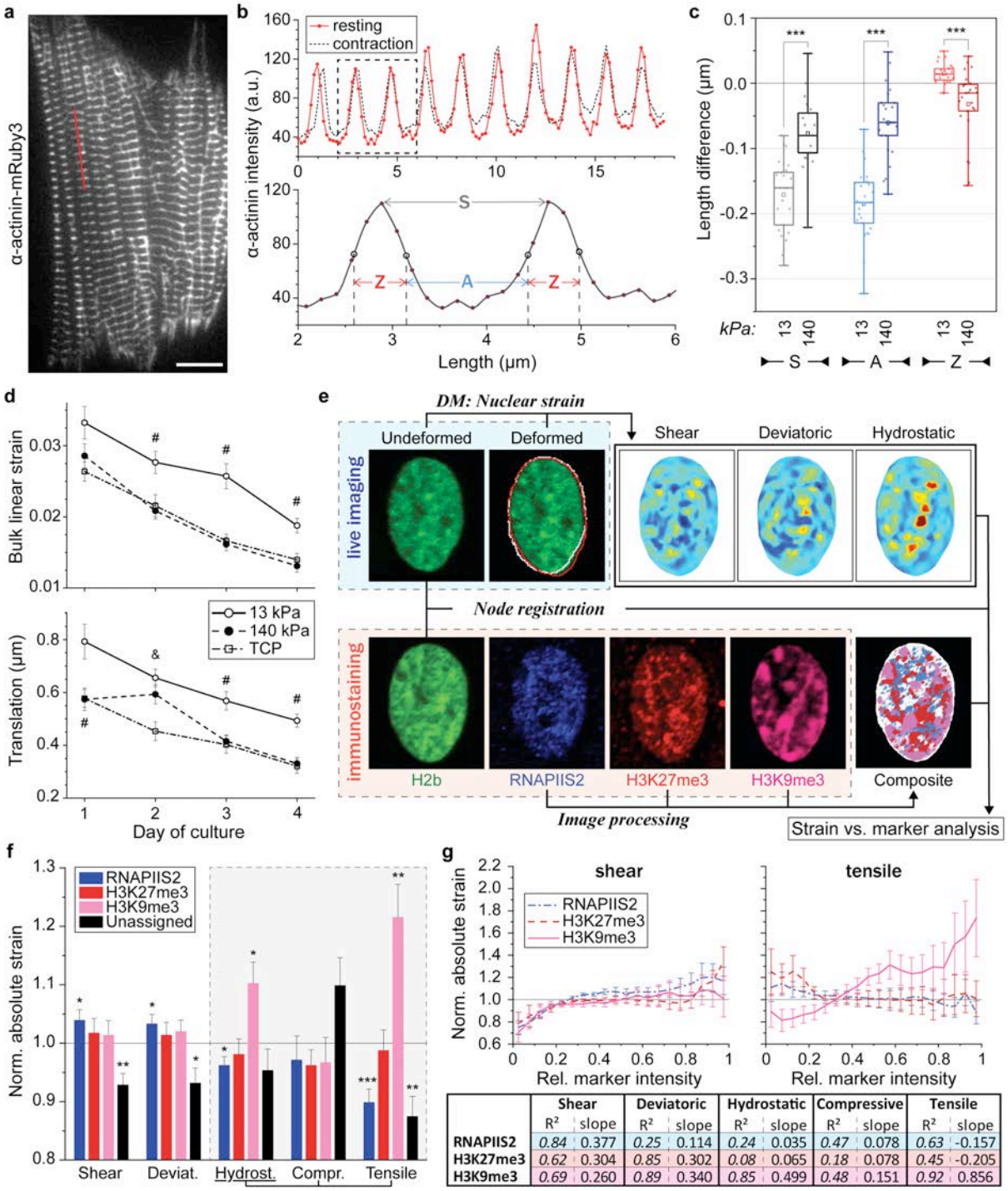

	Shear		Deviatoric		Hydrostatic		Compressive		Tensile	
	R^2	slope	R^2	slope	R^2	slope	R^2	slope	R^2	slope
RNAPIIS2	*0.84*	0.377	*0.25*	0.114	*0.24*	0.035	*0.47*	0.078	*0.63*	-0.157
H3K27me3	*0.62*	0.304	*0.85*	0.302	*0.08*	0.065	*0.18*	0.078	*0.45*	-0.205
H3K9me3	*0.69*	0.260	*0.89*	0.340	*0.85*	0.499	*0.48*	0.151	*0.92*	0.856

Fig. 5. H3K9 methylated chromatin domains are localized to intranuclear subregions with elevated tensile strains during CPC contractions. Cardiac precursor cells (CPC) were isolated from E18.5 H2b-eGFP embryo hearts. **a)** CPCs were infected with an adenovirus expressing fluorescently tagged α-actinin-2 and image stacks during contraction were recorded; scale bar=10 μm. **b)** Top: α-actinin-2 intensity profile, as indicated by a red line in a), before (resting) and during contraction. Bottom: Blow-up of two intensity peaks. Analysis of intensity profiles was used to determine overall sarcomere length (S)

as well as A-band (A) and Z-disk (Z) length. **c)** Difference of sarcomere feature before and during contraction. Cells on stiff (140 kPa) PDMS showed inhibited contraction as overall sarcomere and A-band shortening as well as Z-disk extension was abrogated compared cells cultured on soft (13 kPa) PDMS. n=25; T-Test: *** $p<0.001$. **d)** CPCs were cultured on either soft (13 kPa) PDMS, stiff (140 kPa) PDMS or TCP for four days during which image stacks of beating CPC nuclei were recorded and bulk linear strain and translational movement of nuclei were calculated. Nuclei of cells cultured on soft substrates showed higher bulk linear strain and translational movement compared to stiff PDMS and TCP; Error bars=SEM; n>40; ANOVA ($p<0.05$): # 13 kPa vs. 140 kPa and TCP, & 13 kPa vs. TCP. **e)** Flowchart of intranuclear strain analysis using *deformation microscopy* (DM). Image stacks of CPC nuclei were recorded during contractions. Frames during resting state (undeformed, white outline) were used as template while frames during peak contraction (deformed, red outline) were used as target images to calculate intranuclear strain with high spatial resolution. Cells were then stained for the epigenetic markers H3K9me3, H3K27me3 or actively transcribed chromatin (RNAPIIS2). H2b-eGFP images were used to register nodes between both datasets to analyze the strain occupancy for epigenetically repressed or active nuclear areas. **f)** Absolute strains of nuclear areas that are predominantly occupied by one of the chromatin markers, or none of the markers (unassigned, white areas in composite image in e), were calculated and normalized to the average strain of each nucleus. H3K9me3-marked regions particularly coincided with areas of high tensile strain. SEM; n=20; T-test: * $p<0.05$, ** $p<0.01$, *** $p<0.001$. **g)** Intranuclear strains were analyzed over chromatin marker intensities. Top: Strain vs. intensity plot for shear and tensile hydrostatic strain (see Suppl. Fig. 2 for other strains). Bottom: Linear regression summary from strain vs. intensity plots. Highest R^2 and steepest slope was observed for tensile hydrostatic strains over H3K9me3 intensities. SEM; n=20.

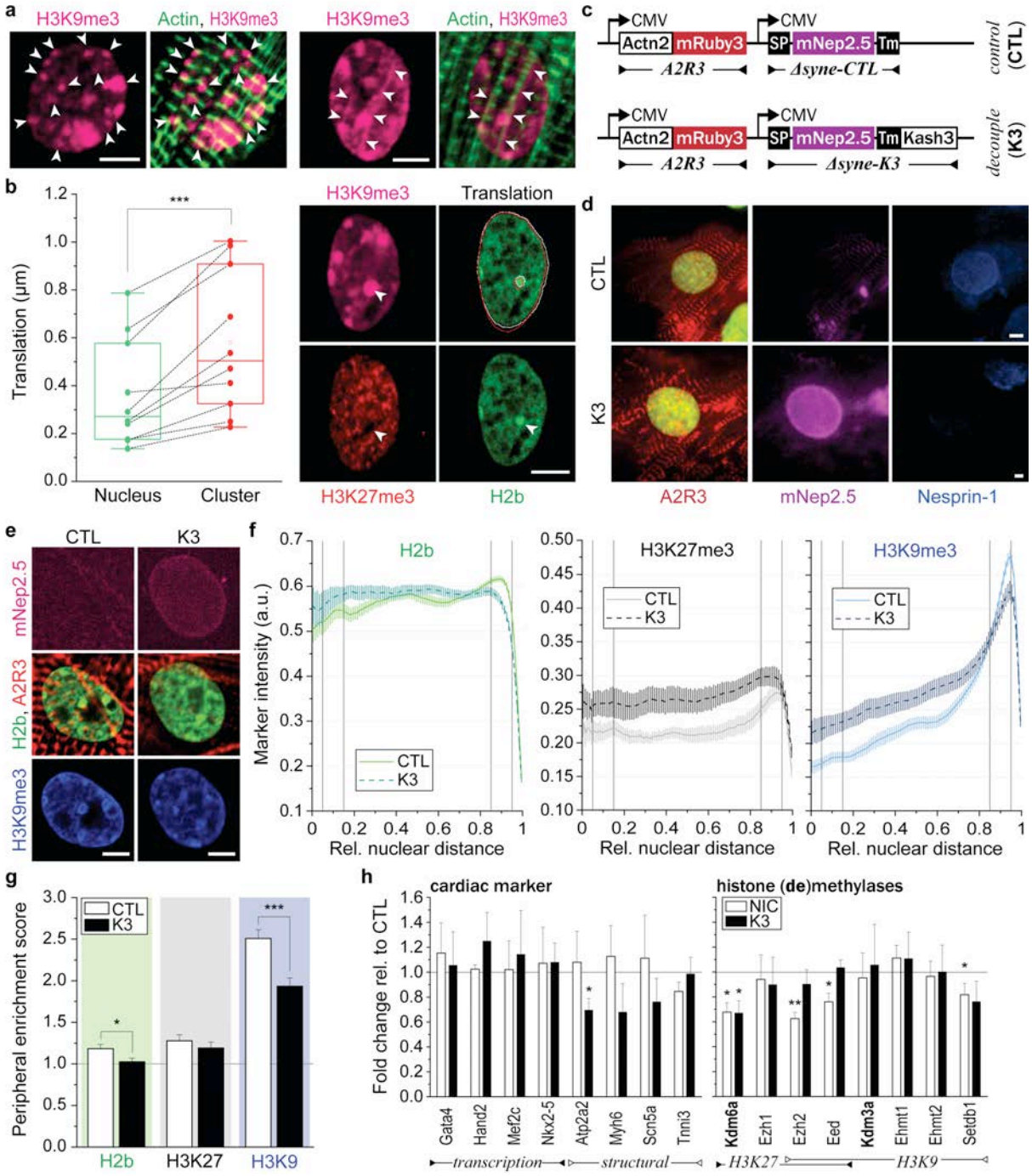

Fig. 6. LINC complex disruption abrogated strain-sensitive relocation of H3K9 methylated chromatin, but not regulation of histone (de)methylases. Cardiac precursor cells (CPC) were isolated from E18.5 H2b-eGFP embryo hearts and cultured on soft (13 kPa) PDMS substrates. **a)** At day two, cells were stained for H3K9me3 and actin. Left: Z-disks of ventral sarcomeres coincide with H3K9me3-rich chromatin clusters (white arrows). Right: Dorsal sarcomere fibers overlap with linear H3K9me3 formations along the major axis (white arrows). **b)** Nuclear image stacks of beating CPCs were recorded on day two of culture and the translation of dense, H3K9me3-rich heterochromatin clusters and overall

nuclear translation were analyzed. Translational movement was higher for heterochromatin clusters than for nuclei during contractions. White and red outlines indicate nuclear and cluster boundary during rest and peak contraction, respectively. n=10; T-Test: *** $p<0.001$. **c)** Adenoviral vectors for LINC disruption. The decoupling vector (K3) expressed a truncated nesprin-3 composed of the transmembrane (TM) and the Kash domain tagged with mNeptune2.5 (mNep2.5) to track nuclear membrane integration. The control vector (CTL) lacked the Kash domain necessary for LINC complexes. Fluorescently tagged α-actinin (*Actn2*) was expressed to identify infected cells. **d)** 24h post transduction, widefield imaging of fixed CPCs infected with the decoupling vector showed successful integration of the truncated Nesprin construct (mNep2.5) into the outer nuclear membrane while no distinct localization was observed for the control vector. Decoupled cells showed disrupted sarcomere fibers, particularly around the nucleus, and immunostaining demonstrated diminished nesprin-1 presence at the nuclear membrane. **e-g)** Infected CPCs were stained for H3K9me3 or H3K27me3 on day two and peripheral enrichment of chromatin was analyzed using a custom MATLAB code. Decoupled cells (K3) showed abolished enrichment of overall and H3K9me3-marked chromatin compared to infected control cells (CTL) while H3K27me3-marked chromatin was similarly enriched. SEM; n=35; T-Test: * $p<0.05$, *** $p<0.001$. **h)** Gene expression analysis of decoupled (K3) or non-infected control cells (NIC) compared to infected control cells (CTL). Expression of structural, but not transcriptional, cardiac genes was reduced in decoupled cells, while expression of histone methylating and demethylating genes remained largely unchanged except for a decrease of *Kdm6a*. SD; n=4; T-Test: * $p<0.05$, ** $p<0.01$. All scale bars=5 µm.

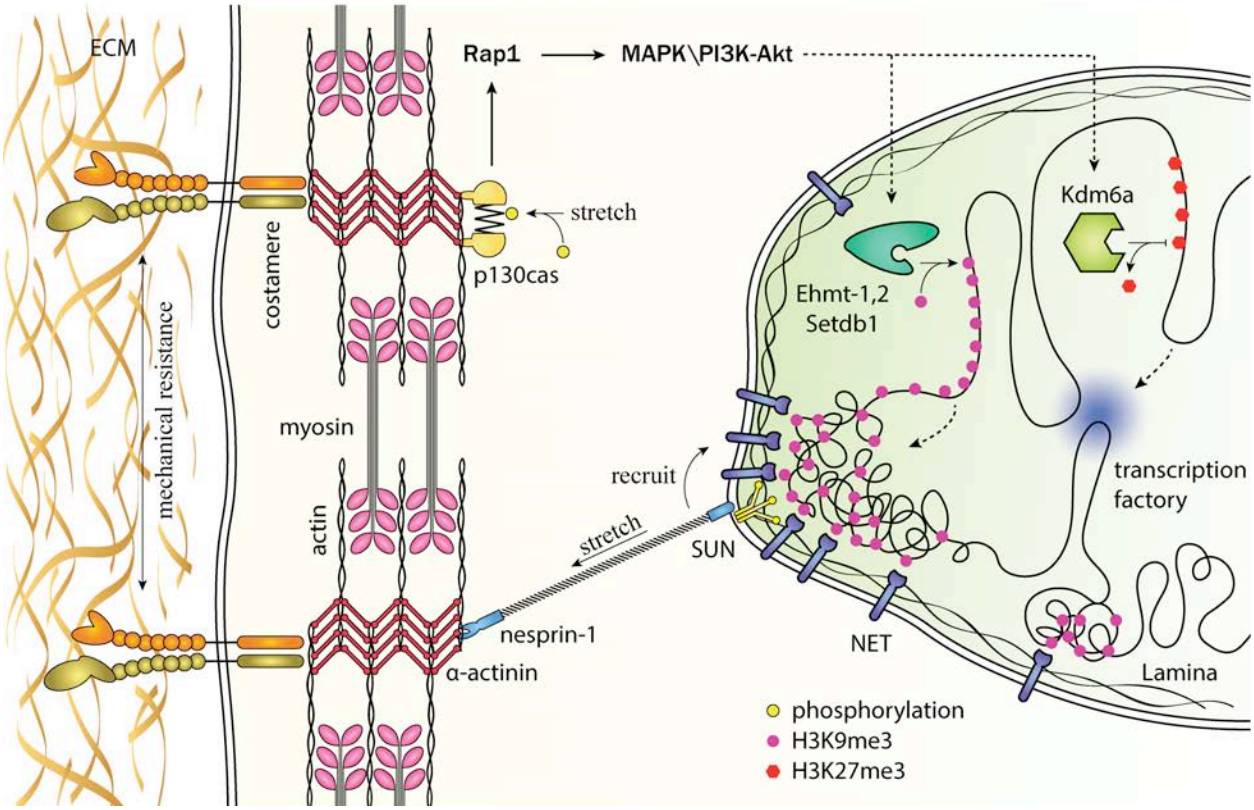

Fig. 7. Proposed model for mechanosensitive reorganization of chromatin and its role during cardiac development. Sarcomere contractions cause a conformational change in α-actinin containing Z-disks and activate the associated mechanosensor p130Cas through phosphorylation of cryptic binding sites. Activated p130Cas mediates a change in epigenetic modifications by increasing H3K9me3 and decreasing H3K27me3 modifications via MAPK/PI3K-Akt. Stretch activation of LINC complexes (SUN + nesprins) directs H3K9me3-marked chromatin to the nuclear border. The segregation of suppressed (H3K9m3-marked) non-cardiac genes to the enzyme-deprived nuclear periphery might prevent it from reactivation and hence stabilizes cardiomyocyte differentiation. Recruitment of nuclear envelope transmembrane protein (NETs) that selectively bind epigenetically-marked chromatin could be a potential mechanism how chromatin is tethered to the nuclear border after rearrangement. The integration of multiple mechanosensitive pathways could be used as a feedback for robust cardiomyocyte differentiation by allowing only cardiac precursor cells with sufficient contractility to become a cardiomyocyte. Inversely, when a change in material properties decreases the contractile work of cardiomyocyte (e.g. through increase of mechanical resistance) suppressed chromatin moves back towards the nuclear center. This might result in the reactivation of cardiac fetal genes and general dedifferentiation of cardiomyocytes observed during cardiac hypertrophy or fibrosis. See also Supplementary Fig. 7.

SUPPLEMENTARY INFORMATION

SUPPLEMENTARY TABLES

Supplementary Table 1. Substrate specificity of differentially expressed histone methylating genes. List of differentially expressed ($p<0.2$) genes between soft and stiff PDMS, as determined by RNAseq, with the GO term association *histone methylation* (GO:0016571). Shown are substrate specificities for mono (1), di (2), tri (3) or any methylation of the respective target histone residue as obtained from either UniProt or AmiGO database. H3K9 residues were amongst the most prevalent substrates.

Gene	***Substrate specificity***	***Source***	***Fold change***	***P-value***
Ehmt1	H3K9me1/2	UniProt	0.847	0.0185
Paxbp1	H3K4me2/3	UniProt	0.751	0.0666
Pwp1	H3K20me3	AmiGO	0.860	0.0797
Setdb1	H3K9me3	UniProt	0.823	0.0830
Rtf1	H3K4me3	UniProt	1.127	0.1119
Setd1a	H3K4me	UniProt	0.670	0.1190
Setd1b	H3K4me	UniProt	0.193	0.1573
Eed	H3K9me, H3K27me	UniProt	0.719	0.1687
Arid4b	H3K9me3, H3K20me3	AmiGO	1.158	0.1881

Supplementary Table 2. KEGG pathway analysis of cardiac precursor cells plated on soft or stiff PDMS substrates. Global gene expression data from RNAseq analysis was used to screen for pathways with enriched differential gene expression using the KEGG database via DAVID. Shortlisted are pathway terms involved in signal transduction cascades (for full list see Supplementary Table 1) as well as the number of genes involved, *p*-values and corrected *p*-value Benjamini-scores using the Benjamini-Hochberg procedure.

Term	Genes#	% total	*P*-value	Benjamini
Signaling pathways regulating pluripotency of stem cells	29	1.2	0.0002	0.0650
Rap1 signaling pathway	35	1.4	0.0050	0.2100
Toll-like receptor signaling pathway	20	0.8	0.0055	0.1800
TNF signaling pathway	20	0.8	0.0120	0.3000
MAPK signaling pathway	37	1.5	0.0210	0.2800
PI3K-Akt signaling pathway	48	2	0.0270	0.3200
Adrenergic signaling in cardiomyocytes	24	1	0.0280	0.3100
HIF-1 signaling pathway	18	0.7	0.0310	0.3300
Cholinergic synapse	19	0.8	0.0340	0.3500
cGMP-PKG signaling pathway	26	1.1	0.0370	0.3300
Insulin resistance	18	0.7	0.0500	0.3600
AMPK signaling pathway	20	0.8	0.0520	0.3700
ErbB signaling pathway	15	0.6	0.0530	0.3700
ECM-receptor interaction	15	0.6	0.0580	0.3700
Neurotrophin signaling pathway	19	0.8	0.0650	0.3800
Estrogen signaling pathway	16	0.7	0.0670	0.3800
Wnt signaling pathway	21	0.9	0.0750	0.4000
VEGF signaling pathway	11	0.4	0.0770	0.4000
Hippo signaling pathway	22	0.9	0.0820	0.4100
Jak-STAT signaling pathway	21	0.9	0.0930	0.4300
Calcium signaling pathway	25	1	0.0960	0.4300

Supplementary Table 3. PCR primers for gene expression analysis.

Gene	Forward	Reward
Gapdh	TGTCAAGCTCATTTCCTGGTATG	GGGATAGGGCCTCTCTTGCT
ActB	GATCAAGATCATTGCTCCTCCTG	AGGGTGTAAAACGCAGCTCA
Gata4	CTCCATGTCCCAGACATTCAGT	GATGCATAGCCTTGTGGGGA
Hand2	CACCAGCTACATCGCCTACC	TCTCATTCAGCTCTTTCTTCCTCT
Mef2c	ACCTCCCAGCTTTGAGATGC	CCATCAGACCGCCTGTGTTA
Nkx2-5	ATTTTACCCGGGAGCCTACG	CAGCGCGCACAGCTCTTTT
Atp2a2	CCGGCTGAAGAAGGAAAAACC	CCACGATTGCATTGGCTACC
Myh6	CTCTGGATTGGTCTCCCAGC	GTCATTCTGTCACTCAAACTCTGG
Scn5a	ATATGTTGAGTACACCTTCACCGC	CGATCACACTGAAGTCTAGCCA
Tnni3	CGTTCTGAGGACTCGTTGCC	TTAAACTTGCCACGGAGGTCA
Kdm6a	TGGAAACGTGCCTTACCTGC	TGAAGCCCCTGAGTGGAGTT
Eed	TGGGCGATTTGATTACAGCCA	GGGTCAGTGTTGTGCATTTGG
Ezh1	TGGATATAGCAAGTCCCCCA	ACATACAGAGCCTTTGCTCCC
Ezh2	TCCATGCAACACCCAACACATA	ACTCCTTAGCTCCCTCCAGAT
Kdm3a	CAGGACAACTGGGACTTGGAG	CCACACACACCTTCAAGTCTTTC
Ehmt1	GCTAAGGGAAGATACACCTATGGC	CACTCTGTTGGTGCCTTCCT
Ehmt2	GAACTCTGGTAGCCTGTCCG	GCTCATCCACAGAGTACGCA
Setdb1	CATACAGCAGCGCAAGAAGC	AGTTAGTCACTTCCCTGGATGC

SUPPLEMENTARY FIGURES

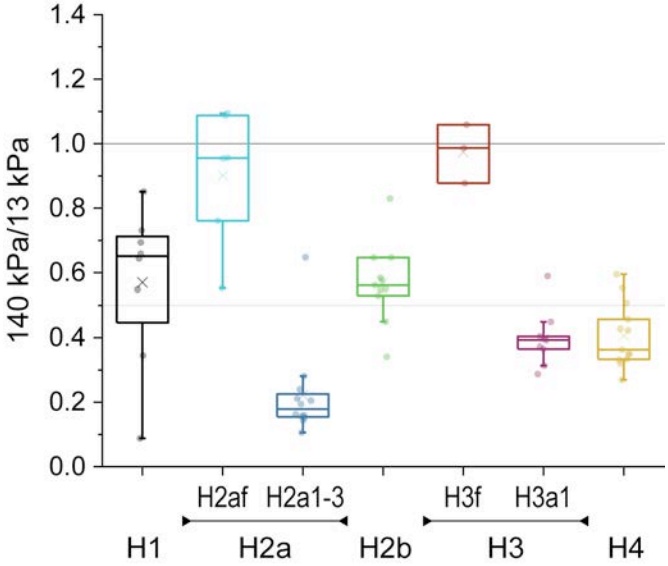

Supplementary Fig. 1. Substrate stiffness effect on histone (sub)family gene expression. Cardiac precursor cells (CPC) were isolated from E18.5 H2b-eGFP embryo hearts and cultured on soft (13 kPa) or stiff (140 kPa) PDMS for four days after which total RNA was collected. RNAseq analysis showed that most histone coding genes were downregulated on stiff substrates, particularly histone family H4, H2a subfamilies H2a1-3 and H3 subfamily H3a1.

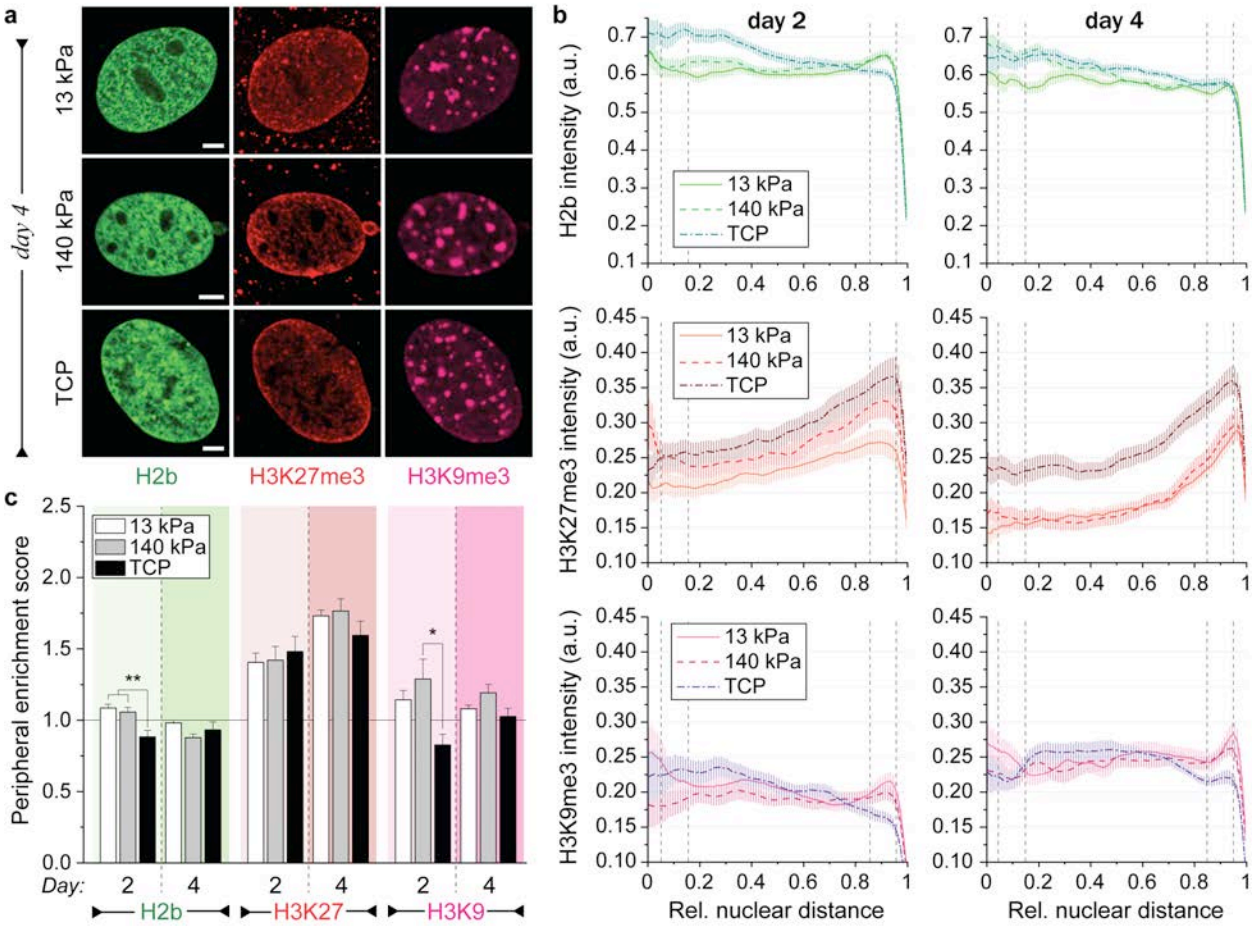

Supplementary Fig. 2. Effect of pathological mechanical environments on chromatin organization in non-contractile CPCs *in vitro*. a) Cardiac precursor cells (CPC) were isolated from E18.5 H2b-eGFP embryo hearts and cultured on either soft (13 kPa) PDMS, stiff (140 kPa) PDMS or TCP for two or four days after which nuclei were stained for H3K27me3 and H3K9me3, scale bars=5 µm **b)** CPC nuclei were evaluated for peripheral enrichment of overall chromatin (H2b) or epigenetically marked chromatin using a custom MATLAB code that analyzed marker intensity with respect to its relative distance to the nuclear center (0=center, 1=periphery). Black lines indicate center and peripheral bin. Error bars=SEM; n≥60. **c)** Enrichment scores for each chromatin marker were calculated as the quotient of intensity of the peripheral bin (0.85-0.95) divided by the center bin (0.05-0.15). Substrate stiffness only minorly affected chromatin organization and enrichment of overall and H3K9me3-marked chromatin remained low while enrichment of H3K27me3-modified chromatin remained high throughout the four-day culture period. SEM; n≥20; ANOVA: * $p<0.05$, ** $p<0.01$.

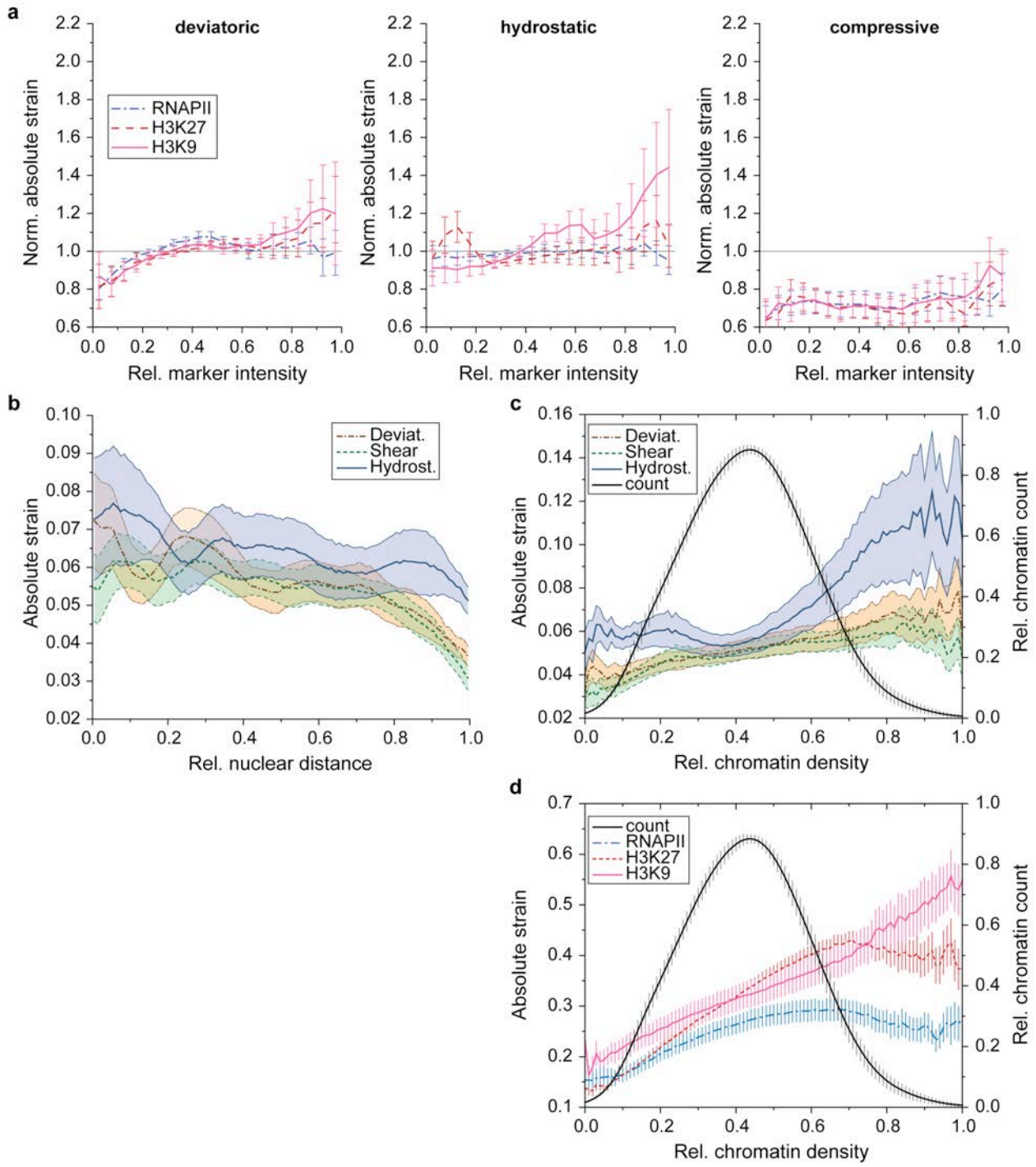

Supplementary Fig. 3. Extended analysis of intranuclear strains during CM contraction. Cardiac precursor cells (CPC) were isolated from E18.5 H2b-eGFP embryo hearts and cultured on soft (13 kPa) PDMS. Intranuclear strain maps were generated via *deformation microscopy* using image stacks of CPC nuclei recorded during contractions. Cells were then stained for the epigenetic markers H3K9me3, H3K27me3 or actively transcribed chromatin (RNAPIIS2). H2b-eGFP images were used to register nodes between both datasets and analyze the strain occupancy for epigenetically repressed or active nuclear

areas. For flowchart and associated data see Fig. 5e-g. **a)** Intranuclear strains were analyzed over chromatin marker intensities. **b)** Intranuclear strains were analyzed over distance to the nuclear center. **c, d)** Intranuclear strains and chromatin marker intensities were analyzed over relative chromatin density based on chromatin intensity. Chromatin density distribution (histogram) is represented as relative chromatin count on the right Y-axis.

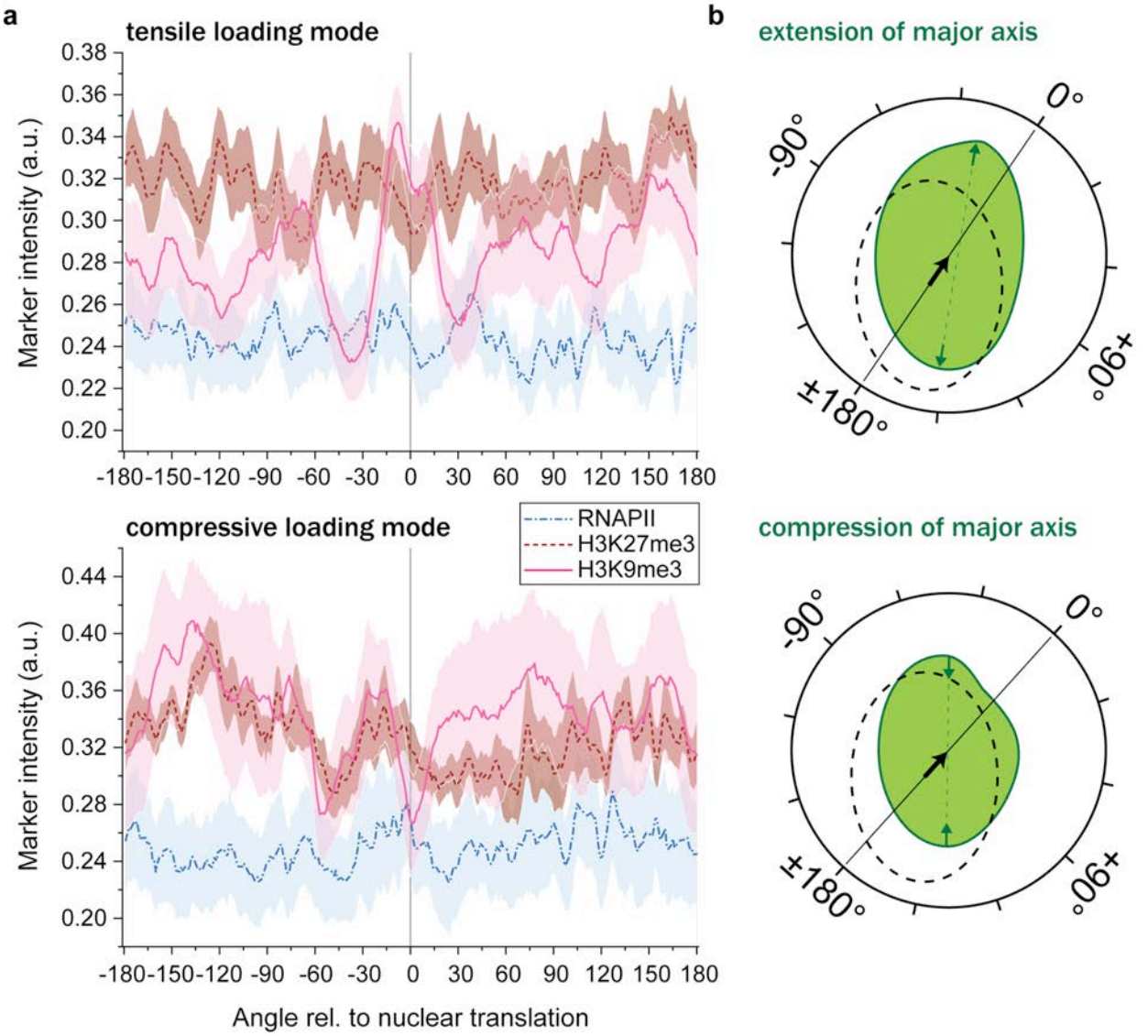

Supplementary Fig. 4. H3K9 methylated chromatin occupancy peaks in the direction of contraction in nuclei with tensile loading mode. a) Cardiac precursor cells (CPC) were isolated from E18.5 H2b-eGFP embryo hearts, cultured on soft PDMS for two days. Image stacks of CPC nuclei were recorded during contractions to determine the direction of nuclear translation. Cells were then stained for the epigenetic markers H3K9me3, H3K27me3 or actively transcribed chromatin (RNAPIIS2). Chromatin marker occupancy was calculated with respect to the angle of the nuclear center with the angle of nuclear translation set to 0°. Cells with extended major axis during contraction (tensile loading mode, n=20) showed a distinct peak of H3K9me3 intensity ±30° around the direction of translation, while cells a decline in H3K9me3 intensity was observed for cells with shortened major axis (compressive loading mode, n=8). SEM **b)** Schematic of angular analysis showing nuclear outlines during resting phase (doted black) and peak contraction (solid green). The black arrow indicates the direction of translation, which defines the 0° point, and green arrows demonstrate extension or compression of the nuclear major axis used to determine the loading mode of cells.

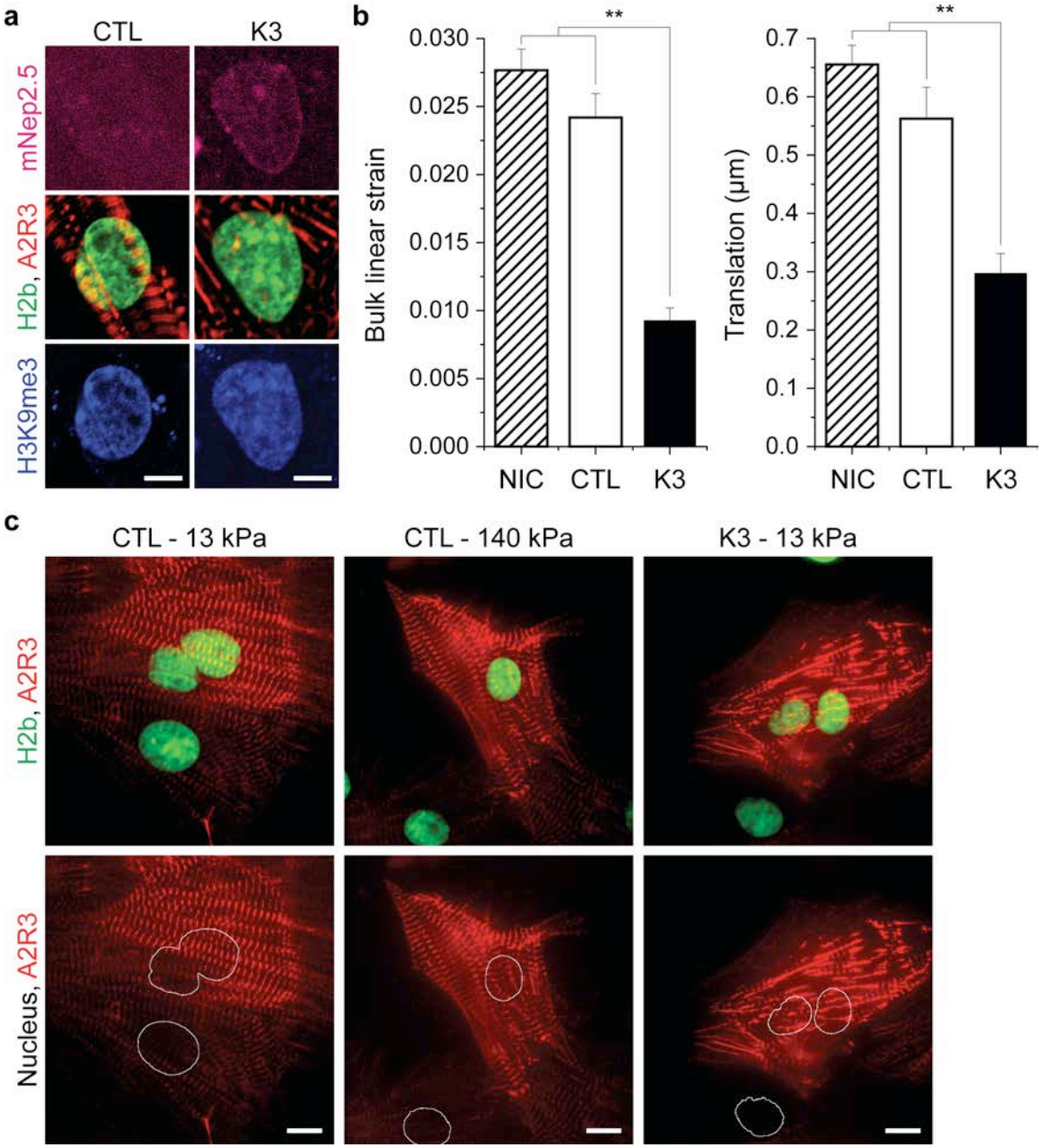

Supplementary Fig. 5. LINC complex disruption inhibits nuclear maturation. Cardiac precursor cells (CPC) were cultured on soft (13 kPa) PDMS. At day 1, cells were infected with an adenoviral vector that disrupted LINC connection, or a control vector. **a**) Cells were stained for H3K27me3 on day two. Decoupled cells (K3) showed abolished enrichment of overall and H3K9me3-marked chromatin compared to infected control cells (CTL) while H3K27me3-marked chromatin was similarly enriched (see also Fig. 6e-g); scale bar=5 µm. **b)** Image stacks of beating CPCs were recorded on day two and bulk linear strain and translational movement of nuclei were calculated. Decoupled nuclei (K3, n=32) showed lower bulk linear strain and translational movement compared to cells infected with the control vector (CTL, n=32) or non-infected control cells (NIC, n=67); SEM; ANOVA: ** p>0.01. **c)** Images of infected

cells plated on either soft (13 kPa) or stiff (140 kPa) PDMS. Decoupled cells show disrupted sarcomere fibers, particularly around the nucleus; scale bar=10 μm.

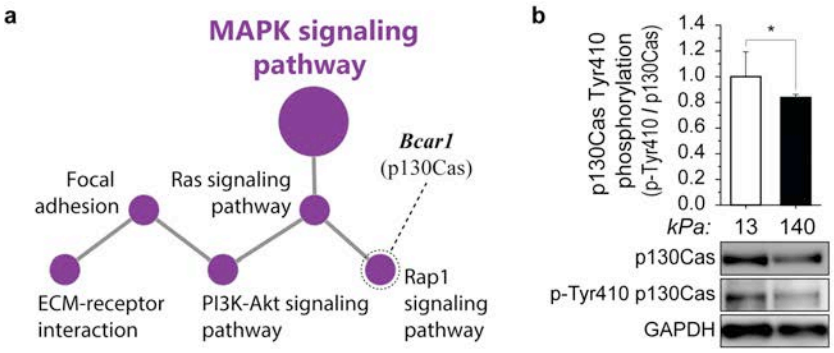

Supplementary Fig. 6. CMs on stiff substrates showed altered MAPK signaling and inhibited stretch-activation of associated p130Cas. CPC were cultured on soft (13 kPa) or stiff (140 kPa) PDMS for four days before RNA or protein was extracted. **a)** Network analysis of global gene expression change revealed alterations in MAPK signaling and associated pathways that play a role in cell-substrate interaction. Rap1 signaling included the downregulation *Bcar1* coding for p130Cas, a mechanosensitive protein located within the Z-disk lattice in CMs. **b)** Western blot analysis of stretch-induced tyrosine 410 phosphorylation in CPCs plated on soft (13 kPa) or stiff (140 kPa) PDMS. SD; n=3; T-Test: * $p<0.05$.

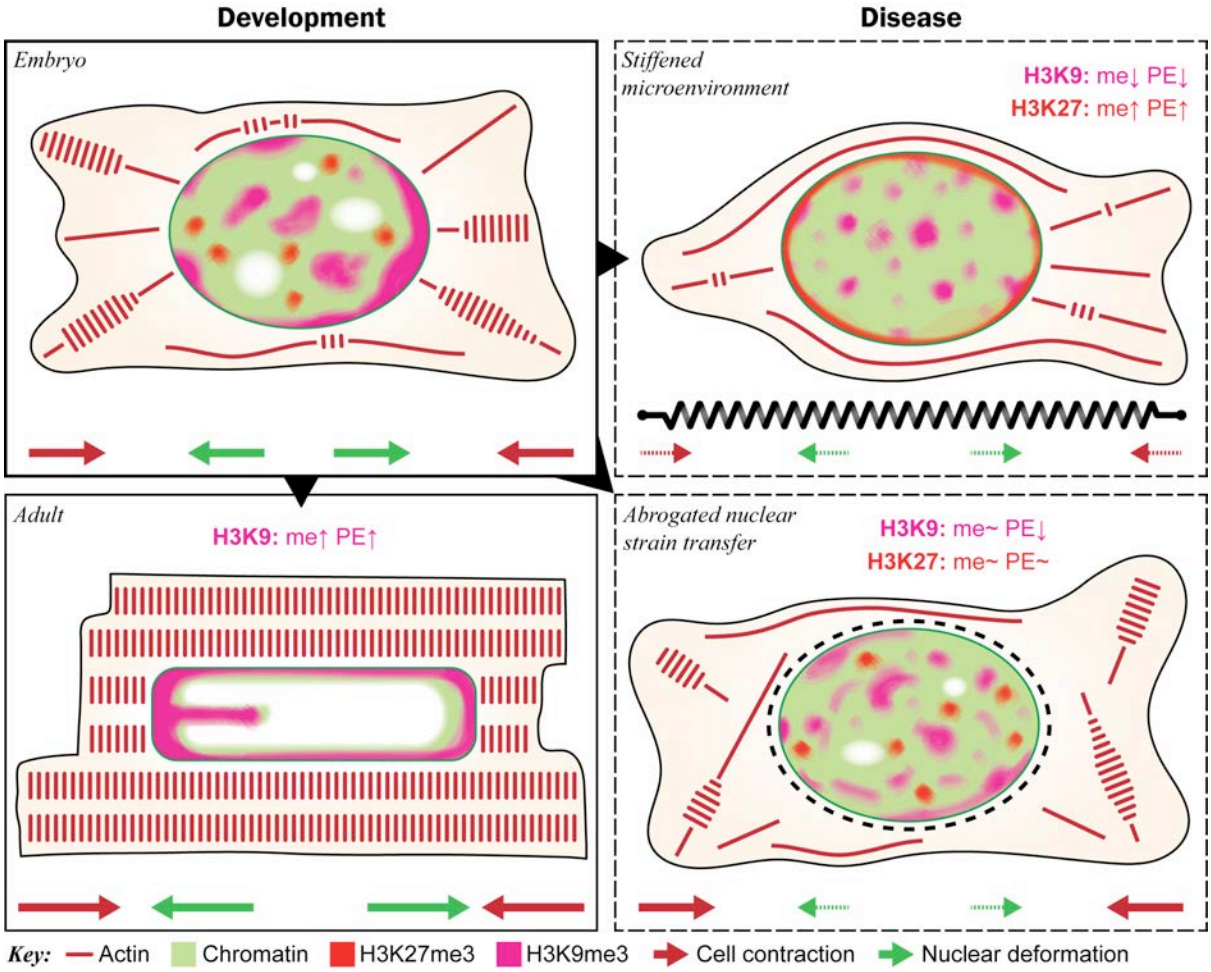

Supplementary Fig. 7. Summary of chromatin reorganization and epigenetic regulation during cardiac development and disease. During development, cell contraction and subsequent nuclear deformation of contractile cardiac precursor cells leads to increased H3K9 methylation (me) and peripheral enrichment (PE) of H3K9me3-modified chromatin. This presumably stabilizes cardiac gene expression by anchoring suppressed non-cardiac genes to the periphery to prevent reactivation. Stiffening of the cardiac micro-environments inhibits cell contraction and nuclear deformation resulting in increased H3K27 methylation and peripheral enrichment instead of H3K9. Abrogation of nuclear strain transfer, independent of cell contraction through disruption of LINC complexes, generally inhibited chromatin reorganization while regulation of methylation remained largely unchanged, suggesting that nuclear mechanosensation primarily affects chromatin reorganization.